UPPSALA
UNIVERSITET

*Digital Comprehensive Summaries of Uppsala Dissertations from the Faculty of Medicine* 930

# Protons, other Light Ions, and $^{60}$Co Photons: Study of Energy Deposit Clustering via Track Structure Simulations

GLORIA BÄCKSTRÖM



ACTA
UNIVERSITATIS
UPSALIENSIS
UPPSALA
2013

ISSN 1651-6206
ISBN 978-91-554-8736-2
urn:nbn:se:uu:diva-206385

Dissertation presented at Uppsala University to be publicly examined in Skoogsalen, Akademiska Sjukhuset, Ing. 78-79, Uppsala, Friday, October 11, 2013 at 09:15 for the degree of Doctor of Philosophy (Faculty of Medicine). The examination will be conducted in English.

**Abstract**

Bäckström, G. 2013. Protons, other Light Ions, and $^{60}$Co Photons: Study of Energy Deposit Clustering via Track Structure Simulations. Acta Universitatis Upsaliensis. *Digital Comprehensive Summaries of Uppsala Dissertations from the Faculty of Medicine* 930. 55 pp. Uppsala. ISBN 978-91-554-8736-2.

Radiotherapy aims to sterilize cancer cells through ionization induced damages to their DNA whilst trying to reduce dose burdens to healthy tissues. This can be achieved to a certain extent by optimizing the choice of radiation to treat the patient, i.e. the types of particles and their energy based on their specific interaction patterns. In particular, the formation of complex clusters of energy deposits (EDs) increases with the linear energy transferred for a given particle. These differences cause variation in the relative biological effectiveness (RBE). The complexity of ED clusters might be related to complex forms of DNA damage, which are more difficult to repair and therefore prone to inactivate the cells. Hence, mapping of the number and complexity of ED clusters for different radiation qualities could aid to infer a surrogate measure substituting physical dose and LET as main predictors for the RBE .

In this work the spatial patterns of EDs at the nanometre scale were characterized for various energies of proton, helium, lithium and carbon ions. A track structure Monte Carlo code, LIonTrack, was developed to accurately simulate the light ion tracks in liquid water. The methods to emulate EDs at clinical dose levels in cell nucleus-sized targets for both $^{60}$Co photons and light ions were established, and applied to liquid water targets. All EDs enclosed in such targets were analyzed with a specifically developed cluster algorithm where clustering was defined by a single parameter, the maximum distance between nearest neighbour EDs. When comparing measured RBE for different radiation qualities, there are cases for which RBE do not increase with LET but instead increase with the frequencies of high order ED clusters.

A test surrogate-measure based on ED cluster frequencies correlated to parameters of experimentally determined cell survival. The tools developed in this thesis can facilitate future exploration of semi-mechanistic modelling of the RBE.

*Keywords:* Proton, light ion, Co-60 photon, track structure Monte Carlo code, clustering patterns of energy deposit, RBE

*Gloria Bäckström, Uppsala University, Department of Radiology, Oncology and Radiation Science, Section of Medical Physics, Akademiska sjukhuset, SE-751 85 Uppsala, Sweden.*



ISSN 1651-6206
ISBN 978-91-554-8736-2
urn:nbn:se:uu:diva-206385 (http://urn.kb.se/resolve?urn=urn:nbn:se:uu:diva-206385)

*A mis amados Pär y David*

# List of papers

This thesis is based on the following papers, which are referred to in the text by their Roman numerals.

I **González-Muñoz G**, Tilly N, Fernández-Varea J M and Ahnesjö A 2008 Monte Carlo simulation and analysis of proton energy-deposition patterns in the Bragg peak *Phys. Med. Biol.* **53** 2857–75

II Fernández-Varea J M, **González-Muñoz G**, Galassi M E, Wiklund K, Lind B K, Ahnesjö A and Tilly N 2012 Limitations (and merits) of PENELOPE as a track-structure code *Int. J. Radiat. Biol.* **88** 66–70

III **Bäcsktröm**$^{\star}$ **G**, Galassi M E, Tilly N, Ahnesjö A and Fernández-Varea J M 2013 Track structure of protons and other light ions in liquid water: Applications of the LIonTrack code at the nanometer scale *Med. Phys.* **40** 064101

IV **Bäcsktröm**$^{\star}$ **G**, Ahnesjö A, Fernández-Varea J M and Tilly N 2013 Spatial energy-deposit patterns generated by light ions and $^{60}$Co-photons in cell nucleus-sized targets *Manuscript*

$\star$ née González-Muñoz

# Contents


1 Introduction ..... 9

2 The physical and biological basis of radiation therapy ..... 13
2.1 Physical basis of radiation interaction with matter ..... 13
2.1.1 Physical properties of light ions ..... 14
2.2 The relative biological effectiveness, RBE ..... 14
2.2.1 Biological properties of light ions ..... 15
2.2.2 The RBE in the clinical context ..... 16

3 The Monte Carlo method in radiation transport ..... 17
3.1 Particle interaction models for track structure simulation ..... 18
3.1.1 Light ions ..... 18
3.1.2 Electrons ..... 21
3.1.3 Photons ..... 22
3.2 Track-segment conditions and particle transport ..... 23
3.3 LIonTrack: a track-structure MC code ..... 24

4 Frameworks to generate and investigate EDs at the subcellular level ..... 26
4.1 Generation of EDs ..... 26
4.1.1 EDs by $^{60}$Co photons ..... 26
4.1.2 EDs by protons and other light ions ..... 29
4.2 Cluster method ..... 30
4.2.1 Cluster concepts ..... 30
4.2.2 Cluster scoring algorithm ..... 32

5 Particle track analysis at the nanometre scale ..... 33
5.1 Secondary electrons: slowing-down spectra ..... 33
5.2 Light ions and $^{60}$Co-photons: Spatial patterns of EDs ..... 34
5.2.1 Distances between EDs for single particle tracks ..... 34
5.2.2 ED clustering ..... 36

6 RBE modelling based on ED clusters ..... 43

7 Summary and Outlook ..... 47

8 Sammanfattning på svenska ..... 49

9 Acknowledgments ..... 51

Bibliography ..... 53

# 1. Introduction

In 1899 the first succesful therapeutic treatment of cancer with ionising radiation was reported (see e.g. Mould and Tai 2002). At first, X-Rays were applied to treat cancer, but soon thereafter tumours were also irradiated with radium sources. Deep seated tumours were difficult to reach by these radiation qualities that would deposit a lot of energy in healthy tissues. By 1946, Wilson pointed out that proton radiation could aid to concentrate the energy deposition to the tumour due to the behaviour of protons interacting with matter (Wilson 1946). The first treatments with proton beams started at the Lawrence Berkeley Laboratory (LBL) in California (1954) (Tobias *et al* 1956) and at the Gustaf Werner Institute in Uppsala (1957) (Falkmer *et al* 1962). In the 80's clinical trials were carried out with high-LET radiation qualities such as neon ions at the LBL and negative pions at e.g. Los Alamos National Laboratory (LANL). Trials with helium ions at the LBL in Berkeley (USA), and with carbon ions at the Gesellschaft für Schwerionenforschung (GSI) in Darmstadt (Germany) and at the Heavy Ion Medical Accelerator (HIMAC) in Chiba (Japan), among others, were more successful than the early trials (as described in the review by Schardt *et al* 2010).

As proton and ion therapies are being consolidated, with more than hundred thousand patients treated worldwide at the end of 2012, about forty new facilities are proposed or under construction (PTCOG, 2013). For instance in Scandinavia, Skandionkliniken (Uppsala, Sweden), the first hospital based facility for proton therapy is being built and the first patient is expected to be treated in 2015 (Skandionkliniken, 2013). Also, a Danish National Center for Particle Radiotherapy in Aarhus (Denmark) is planned and might be operative in 2017–2018 (DSMF, 2013). The enhanced availability of particle therapy has motivated a large number of investigations to improve treatment outcome. These range from research on beam delivering techniques (e.g. Bues *et al 2005*, Safai *et al* 2008, Kimstrand 2008, Lorin 2008) and dosimetric analysis (e.g. Medin 1997, Thiansin Liamsuwan 2012), to radiobiological studies concerned with damage and repair to the DNA (e.g. Jeggo 1998, Jakob *et al* 2002, Campa *et al* 2004, Karlsson 2006), the relative biological effectiveness (RBE) of particle therapy (e.g. Belli *et al* 2000, Tilly 2002, Elsässer *et al* 2008, Nikjoo *et al* 2008), and the biological optimization of treatment planning (e.g. Johansson 2006, Kempe 2008, Tobias Böhlen 2012).

In radiotherapy, ionising radiation (photons, electrons, protons or other light ions[1]) deposit a 'sufficient' amount of energy in the tumour so as to sterilize the cancer cells therein. Simultaneously, the absorbed dose (mean energy imparted per mass) in normal tissues should be minimized to spare them. The large experience accumulated with conventional radiotherapy, where the tumour is irradiated by high-energy photons or electrons, has led to the knowledge of effective dose levels to treat various cancer types. Unfortunately, most radiation modalities deposit some amount of energy in the normal tissues. However, protons and other light ions deposit most of their energy at the end of their paths (further details are given in the next chapter) which allows to minimise the energy deposited in healthy tissue. Light ions also have an enhanced biological effectiveness to damage the cells, i.e. a lower physical dose than given for photon irradiation results in the same biological effect (for a certain level of cell survival, base mutation, etc.). The variation of the relative biological effectiveness (RBE) with radiation quality (i.e. particle type and energy) does not univocally depend on the higher linear energy transfered (LET) of light ions (Kraft 2000). Actually, the RBE variation with radiation quality is still not fully understood. Nevertheless, acquired clinical experiences together with results from physical and radiobiological studies suggest that protons and other light ions of low atomic number ($Z_p < 7$) are the most suitable for particle therapy (Kraft 2000, Kempe *et al* 2006). Depending on the tumour depth, size, cell type, oxygen status and its proximity to organs at risk, optimal selection of ion species could be advantageous owing to their specific physical properties and different RBEs. Hence, a better understanding of the RBE should help to optimize therapeutical treatments and improve their outcome.

The absorbed dose to the tumour is a macroscopic measure of the imparted energy in the volume of interest. However, energy is imparted by many discrete interactions (on the order of $10^5$ per cell at clinical dose levels) in which the ionizing particle loses energy. The location of each interaction is called the transfer point and the energy deposited at the transfer point is the energy deposit[2] (ED) (ICRU 1998). The local distribution of EDs is assumed to play a role in the variation of the RBE (Kraft 2000). Close EDs within the DNA structure might inflict complex forms of DNA damage, which are associated to a decrease of the repair capacity of the cell (Stenerlöw *et al* 2002), and consequently influence cell survival. Hence, the characterization of the spatial ED patterns (e.g. the quantification of ED clusters (groups of EDs), and their cluster order (number of EDs in the cluster), and sizes (geometrical extension), etc.) in the irradiated medium at a nanoscopic level might help to

[1]We adhere to the terminology recommended by ICRU and IAEA (Wambersie *et al* 2004), where light ions include atomic projectiles with atomic number from 1 to 10, i.e. protons, alpha particles, and other ions up to neon.

[2]The energy deposit is employed throughout this work to refer to both the transfer points and the amount of energy deposited.

better explain and evaluate the mechanisms behind the different RBE values. In particular, RBE might be better predicted through a function that utilizes clustering properties of the EDs, rather than physical absorbed dose and LET. This hypothesis relies on the assumption that the irradiation target is the DNA content of the cell, instead of other cellular structures.

The DNA carries the genetic information responsible for the functioning, growing and reproduction of the living organisms. The DNA was first isolated in 1869 (see e.g. Dahm 2008), but it was not before 1953 that Watson and Crick proposed a model for its structure, a double-helical chain of nucleic-acids and peptide backbones. The chain is about 2 nm wide and each nucleic-acid is 0.33 nm long. When the DNA chain is broken or otherwise damaged, for instance due to radiation-induced EDs, the biological mechanisms of the cell activate repair processes and prevent it from reproducing. Depending on the severity of the damage, apoptosis (cell death) can also be induced. Theoretical investigations devoted to the analysis and quantification of the severity of the DNA damage have proposed classifications according to the amount of deposited energy, the site of deposition (in the bases or in the double-chain) and the distances between deposition sites within the DNA. For instance, Nikjoo *et al* (1999) suggested that an ED larger than 17.5 eV would be necessary to cause a single strand break (SSB), and that two SSBs within a distance less or equal to 10 base pairs should yield a double strand break (DSB). It was thought that DSBs were responsible for the more efficient cell sterilization ability of the more densely ionizing radiations. However, survival differences after proton and carbon ion irradiation are not well correlated to the yield of DSB formation, neither after allowing for repair (Stenerlöw *et al* 2002). These differences might be due to the formation of more complex forms of damage, like multiple DSBs within a short range. The frequency distribution of DNA fragments and their lengths can be measured 'in vitro' and 'in vivo' after irradiation with various radiation qualities. The lengths of the fragments are larger for the sparsely ionising radiation (e.g. photons) than for the light ions. Some studies have indicated that the higher presence of complex DNA damage types, which increases with the atomic number of the projectile, could favour cell pathways inducing apoptosis, instead of those allowing for repair (see e.g. Brahme 2004). In particular, the distribution of distances between ED sites, and hence the ED cluster formation, influences the efficiency of the cell to repair DNA damage (Bigildeev and Michalik 1996, Ottolenghi *et al* 1997, Nikjoo *et al* 1999), consequently altering the probability of the cell to survive and reproduce. Hence, ED patterns should be characterized at the nanometre scale, due to both the size of the targeted biological structures and the stochastic nature of the ED events (Goodhead 2006, Grosswendt 2006). Whereas this kind of data is just partially or indirectly available from experiments, track-structure Monte Carlo (MC) codes (Ottolenghi *et al* 1997, Emfietzoglou *et al* 2003, Champion *et al* 2005, Champion and Loirec 2006, Nikjoo *et al* 2006) are a powerful tool for generating the ED patterns in e.g. liquid water for any

radiation quality. The reliability of the patterns of EDs depends on the accuracy of the interaction models between the particle and the water molecule. The properties of clusters of EDs generated with precision at the nanometre scale can be quantified, and eventually correlated to cell survival and other endpoints.

The scope of this thesis is to characterize the spatial patterns of EDs for different radiation qualities via track-structure simulations, and to explore ED cluster quantities that could be used to predict radiation response better than the absorbed dose. To accomplish these goals, we followed the procedure outlined below:

1. To develop a simple MC tool to analyse spatial and energetical properties of the secondary electrons ejected by proton impact in liquid water. We quantified the contribution of the primary proton to the total energy deposited along the track (paper I).

2. To develop a MC track-structure tool for the transport of protons and other light ions in liquid water with accuracy at the nanometre scale (paper III). We highlighted the limitations of the physics models included in the PENELOPE package for the present purposes and outlined a solution (paper II). We also studied the distribution of distances between neighbouring EDs for single ion tracks (paper III).

3. To develop the framework for the investigation of the spatial patterns, and specifically clustering capabilities, of the EDs generated in cell nucleus-sized targets by both light ions and $^{60}$Co photons (paper IV).

4. To undertake a general examination of the ED clustering by various light ions and energies and by a reference radiation quality, $^{60}$Co. We quantified frequencies of ED clusters and related properties in cubic targets of 10 $\mu$m side for proton, helium, lithium and carbon ions in the energy range of about 1–20 MeV/u (paper IV).

5. To quantify the frequencies of cluster orders of EDs by radiation qualities for which RBE is experimentally measured. We searched for a correlation between the cluster order frequencies and published RBE values.

# 2. The physical and biological basis of radiation therapy

## 2.1 Physical basis of radiation interaction with matter

Ionising particles traversing a biological medium undergo a series of interactions that modify the particles' initial states and may result in energy deposition in the medium. These interactions can be divided in two groups: inelastic and elastic. Inelastic interactions are those associated to energy losses (and may also include directional changes) of the particle, i.e. local energy depositions or energy transfered to secondary particles. The elastic ones merely change the particle's trajectory. The collection of interactions produced along the path is commonly refered to as the history or the track of the particle.

The mean distance travelled by a particle between two interactions is given by the mean free path,

$$\lambda = (\mathscr{N}\sigma)^{-1}, \tag{2.1}$$

where $\mathscr{N}$ is the molecular density of the medium and $\sigma$ the cross section; $\lambda^{-1}$ is the probability of interaction per unit path length. The range is the total distance travelled by the particle until it has lost its energy.

Along its travel, the particle looses an average amount of energy per unit path length, that varies with the properties of the material and of the particle itself (type and energy). This quantity is the (linear) stopping power, $S = -\mathrm{d}E/\mathrm{d}x$, for charged particles; the equivalent for photons is the energy-transfer coefficent, $\mu_{\mathrm{tr}}$. The stopping power has two contributions; the electronic stopping power $S_{\mathrm{el}}$ caused by the Coulomb interaction with the electrons of the target medium, and the nuclear stopping power $S_{\mathrm{nuc}}$ due to the Coulomb collisions with the nuclei, in which recoil energy is imparted to the atom as a whole. This last term contributes very little to the total $S$, becoming important only at very low energies and increasing with the charge of the projectile. A common practice in medical physics is to adopt the stopping powers recommended by the International Commission on Radiation Units and Measurements (ICRU). Above about 50 MeV/u, nuclear inelastic scattering also contributes to the stopping of the particles and becomes larger with increasing particle energy (up to $\sim 30\%$). The restricted stopping power or linear energy transfer (LET), $L_\Delta$, represents the locally transferred energy, i.e. energy lost by the primary charged particle in electronic collisions in a track length $\mathrm{d}l$ minus the energy carried away by secondary electrons which kinetic energy is larger than $\Delta$ (ICRU 1998). For $\Delta = \infty$, LET equals $S$. In micro- or nanometre applications it is common to express both quantities in keV/$\mu$m or eV/nm.

The energy deposited in a single interaction is called energy deposit, ED, and the sum of all EDs in a given volume is the energy imparted, $\varepsilon$, to that volume. The quotient of the energy imparted to the matter in a given volume by the mass $m$ of the volume is the specific energy, $z$. The mean energy imparted per unit mass is the absorbed dose, $D$, and it is usually expressed in grays (Gy) (ICRU 1998). In radiotherapy, the absorbed dose to the tumour is often delivered in fractions of about 2 Gy. The stochastic character of the radiation interactions causes large fluctuations of $z$ for small volumes in the scale of the DNA. Hence, the significance of analysing the spatial patterns of EDs generated by different radiation qualities at the nanometre level.

### 2.1.1 Physical properties of light ions

Protons and other light ions have physical and biological properties that help concentrating the absorbed dose to the tumour while minimizing the doses to the normal tissues. In particular, they have a large rate of energy loss at the end of their range, in the so-called Bragg peak (BP). The magnitude of the BP increases at first with the atomic number of the projectile due to less straggling, but diminishes partially for ions with large atomic number ($Z_\mathrm{p} > 10$) as the probability of nuclear fragmentation increases. Nuclear fragmentation processes induce a higher energy deposition beyond the BP, the so-called fragmentation tail. A lateral broadening of the dose distribution also occurs with decreasing atomic number, caused by enhanced multiple scattering. Light ions are completely stripped of their electrons when they travel with high energies, but capture and loss of electrons from the medium contributes to the stopping at specific energies below $\sim 0.5$ MeV/u. Hence, during most of the therapeutic energy interval, the light ions move as bare charged particles.

## 2.2 The relative biological effectiveness, RBE

The RBE is defined as the ratio of a reference radiation quality (X-rays or most commonly $^{60}$Co $\gamma$-rays) dose ($D_\mathrm{ref}$) to particle dose ($D_\mathrm{p}$) to produce the same biological or clinical effect level (EL) for a given endpoint,

$$\mathrm{RBE}(\mathrm{EL}) = \frac{D_\mathrm{ref}(\mathrm{EL})}{D_\mathrm{p}(\mathrm{EL})}\,. \tag{2.2}$$

The RBE has been observed to depend on a number of variables, such as particle type, LET, absorbed dose, cell line, repair capacity of the cell, oxygenation status and the biological or clinical endpoint (Kraft 2000). DNA damage and cell survival are typical examples of endpoints.

The increased ionisation density of light ion tracks as compared to conventional therapy (photons and electrons) might cause an increase of the induced

complex types of DNA damage, that are more difficult to repair (Stenerlöw *et al* 2002), and consequently yield a higher RBE for light ions.

### 2.2.1 Biological properties of light ions

The higher the energy of a light ion, the larger the mean free path between interactions and the lower its LET. Indeed, the ejected secondary electrons can have larger energies with increasing projectile energy. Therefore, the inelastic scattering events occur on average far away from each other, thus generating a spatial pattern of EDs which more resemble sparsely ionising radiation. On the other hand, the lateral scattering of the electrons diminishes at higher LETs for the same particle, and consequently the track becomes narrower. The density of ionising events and the RBE increase along the path with increasing LET. However, different RBE maxima are measured for different particles and these maxima occur at different LETs for different particles (see figure 2.1). Hence, the RBEs are different for particles with the same LET. This implies that the LET is not a particularly accurate indicator for the RBE. Instead, the clustering properties of EDs (number and relative location between EDs) might explain such variations (see e.g. Goodhead 2006, Schardt *et al* 2010).

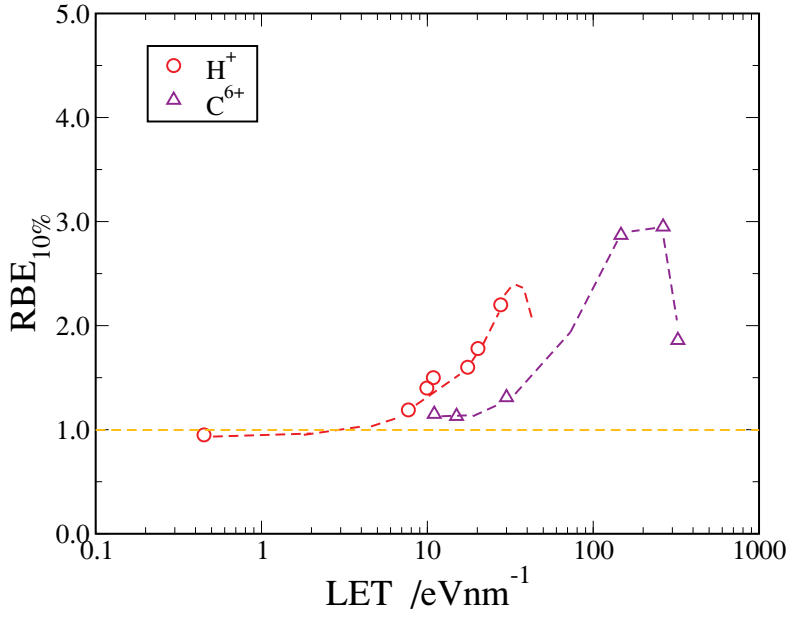


*Figure 2.1.* Experimentally measured RBE values for cell survival for irradiation by protons (circles) and carbon ions (triangles) of various LET for V79 cell lines. Results correspond to data by Belli *et al* (1998) and Folkard *et al* (1996) for protons; and Weyrather *et al* (1999) for carbon ions.

Different cell lines have a different cell survival curve after irradiation with the same radiation quality and absorbed dose (Kraft *et al* 1992). The larger the repair capacity of the cell line for the reference radiation, the larger the RBE effect when LET is increased. The RBE maximum arises at about the same LET but presents different magnitudes when varying the endpoints within the same cell line.

### 2.2.2 The RBE in the clinical context

The RBE for protons in current clinical routine is generally set to 1.1 (ICRU 2007), whereas carbon ions have larger values of about 3–4 (Schardt *et al* 2010). The RBE variations should be carefully accounted for in treatment planning as suggested e.g. by Kraft (2000), Tilly (2002) and Paganetti and Goitein (2000). The RBE dependence on the distinct tissue repair capability should also be considered. For instance, slowly growing tumours have in general a large repair capacity and their treatment has the potential to become relatively more efficient with increasing atomic number of the radiation quality. The physiological conditions of the tumour are also an important component for treatment outcome. Hypoxia is a typical condition that causes radioresistance of the tumour, due to a low level of radiation induced free radicals in the cell. It has been suggested that hypoxic tumours could have a better response to treatments with ions heavier than protons (Brahme 2004) owing to an increased efficiency of the cell sterilization caused by the larger and more localised EDs in the cell. Indeed, the enhanced cell sterilization causes the remaining cells in the tumour to have more oxygen available, getting them back to other phases of the cell cycle where they are more radiosensitive. The RBEs are larger for light ions heavier than protons and hence, the RBE variations have to be included in treatment plannings to produce an homogeneous biological effect in the whole target volume (Schardt *et al* 2010). RBE variations are also introduced when utilizing particles of different energies to spread out the Bragg peak within the target volume. The 1.1 ratio used in proton therapy for the RBE does not account for the increased RBE at the distal end of the BP, where a rise up to 1.3–1.4 could appear (see Tilly 2002 and references therein).

Models currently used in ion therapy (e.g. the HIMAC approach and the LEM model, see Schardt *et al* 2010 for a review) do not resolve all the RBE dependences. A better understanding of the mechanisms behind RBE variations could help to develop a model that predicts such variations, and be consequently applied in treatment planning. The characterization of the spatial patterns of EDs in the irradiated medium at a subcellular level can potentially facilitate the assessment and understanding of the mechanisms behind RBE variations.

# 3. The Monte Carlo method in radiation transport

The energy loss mechanisms of ionising radiation when traversing biological media need to be considered for investigations of ionization patterns at the nanometre scale. The Boltzmann transport equation can be solved for continuous phase space quantities given an interaction model, but it will not yield any information on the texture of ionization patterns and is intricate to apply for general geometrical structures. Alternatively, analytical expressions with some approximations on the electron energy and angular distribution of secondaries can be used to model quantities like the radial dose distribution. The main drawback is that they provide only partial descriptions. MC methods are suitable for problems with many independent variables, and can be set up to handle also complicated geometries. In radiation transport situations, random numbers are employed to simulate the history of each particle. In this way, samples of interaction location patterns are intrinsically produced. Hence, with proper interaction models (i.e. sets of cross section data) and sampling algorithms, the ED patterns of various radiation qualities can be generated with precision down to the nanometre scale.

MC particle transport codes can be classified in three groups, according to the transport algorithm type (Berger 1963, Salvat *et al* 2008). 'Event-by-event' codes simulate in detail each interaction occuring in the medium, being usually suitable for micro- and nano-dosimetric applications (provided the reliability of the input physics data included in the code). The class I ('condensed history') strategy groups the effect of various interactions in one simulation step that represents the change of direction and energy loss of all these collisions. Class II ('mixed simulation') combines the change of direction and energy loss of 'soft' collisions in one step but simulates in detail hard events (i.e. those events with an angular deflection or an energy loss larger than given cutoffs). Codes that have recourse to class I or class II simulations provide a description of the phenomena occurring in the target that is macroscopically correct, and permit the transport of the projectiles in large volumes within a resonable CPU time unlike the more time consuming event-by-event codes.

Event-by-event MC codes utilize the probability of interaction of one particle, the total cross section (TCS), to sample the length of the step that the projectile will travel and the type of interaction that it will undergo. Besides, the kinematical variables from any emitted secondary are sampled: from the singly differential cross section SDCS ($\mathrm{d}\sigma/\mathrm{d}\varepsilon$), the energy; or from the dou-

bly differential cross section DDCS ($d^2\sigma/d\varepsilon d\Omega$), both the energy and the angle. These sets of data are calculated from physics models for the interaction between the projectile and the target atoms or molecules. Their degree of sophistication, accuracy and reliability depend on the assumptions on the projectile-target potential representing the interaction, and the initial and final states of the projectile and the outgoing particles. MC codes with event-by-event simulation scheme provide a detailed description of the particle track and hence are often called track-structure codes.

In the next section, both the main assumptions and the valid energy regimes of models dealing with the interaction of particles in liquid water are briefly described (cf. papers I–III). These models are chosen so as to be suitable for nanometric analysis, where often liquid water is the surrogate for biological medium. Section 3.2 discusses transport conditions (cf. papers I, III); and section 3.3 presents the MC track-structure code developed in this project, LIonTrack (cf. paper III).

## 3.1 Particle interaction models for track structure simulation

### 3.1.1 Light ions

Ionisation is the interaction channel accounting for most of the energy deposited by protons and other light ions in liquid water. However, excitations might contribute to a maximum of 10%, depending on the particle type and energy. The energy lost by inelastic nuclear interactions, not accounted for in this work, might become relatively important for large energies of the particle ($E/M > 50$ MeV/u).

Elastic scattering of the light ions is disregarded here, and hence the ion path is assumed to follow a straight trajectory. This is a good approximation for investigations of a 'short' segment of the track (with a length that is much smaller than the ion range).

**Excitation**

The excitation model by Dingfelder *et al* (2000) provides differential (and total) cross sections for the excitation of a water molecule by proton impact for both the low- and high-energy regimes (from about a few tens of eV to a few tens of MeV). The model gives parameters for the most relevant excited states of the water molecule that join the semi-empirical approach of Miller and Green (1973) for low-energy protons with the Born approximation at high energies. In Miller and Green's model the excitation cross sections for electrons are scaled to those for protons as a function of the particles speed. In turn, the excitation cross sections for protons can be scaled to those of heavier charged particles with the square of the effective charge of the ion.

**Ionisation**

The Continuum-Distorted-Wave (CDW) formalism is currently the state-of-the-art for calculating the DDCS for the ionisation of a water molecule by ion impact. The effect of the electrostatic field created by the target electrons on both the projectile and the emitted particle is mathematically described by means of distorted waves. The final expressions of this formalism are however very difficult to compute. Assumptions on the initial state of the target electrons derives in the eikonal-intial-state approximation or CDW-EIS model, which leads to expressions for the DDCSs that are much more tractable. The binding energies of the molecular orbitals of the target medium are implicit parameters of the CDW-EIS formalism. The DDCSs of water vapour can also be calculated with the CDW-EIS model by replacing the binding energies for liquid water with the values for water vapour. Thus, the CDW-EIS theoretical prediction can be compared to experimental values. Values of the DDCS as a function of the angle for various energies of the ejected electron are displayed in figure 3.2 for 6.0 MeV/u $He^{2+}$ projectiles. A more extensive comparison between theoretical and experimental values for DDCSs, SDCSs and TCSs is presented in paper III.

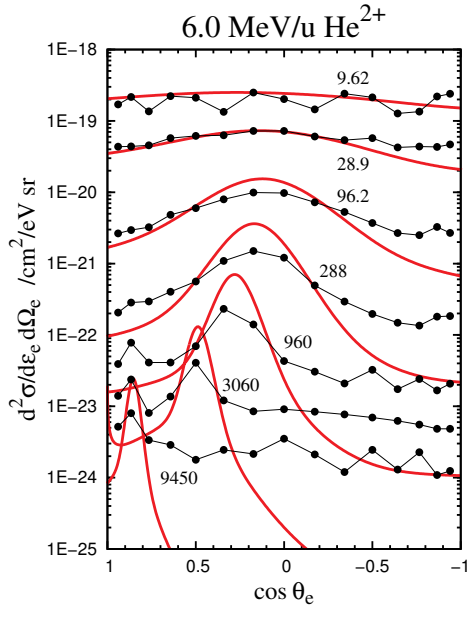


*Figure 3.1.* DDCSs for 6.0 MeV/u $He^{2+}$ ion impact on water vapour. The kinetic energies of the ejected electron are 9.62, 28.9, 96.2, 288, 960, 3060 and 9450 eV (top to bottom). The continuous curves are theoretical predictions of the CDW-EIS, whereas the symbols (joined by segments) correspond to measurements by Ohsawa *et al* (2005).

The DDCS for 1–20 MeV/u protons can alternatively be calculated with the Hansen–Kocbach–Stolterfoht (HKS) model (Stolterfoht *et al* 1997, ICRU 1996). The HKS model is based on the first Born approximation and, unlike the CDW-EIS formalism, describes the active electron with a simple screened hydrogenic wave function for the initial state and with a plane wave for the final state. The shape of the curve for the HKS DDCS reproduces the experimental data in liquid water correctly, but the energy loss by the protons along a track segment is somewhat smaller than the electronic stopping powers recommended by ICRU Report 49 (ICRU 1993). A rescaling factor applied on the HKS TCS compensates for this difference (cf. paper I).

Figure 3.3 displays the electronic stopping power of $H^+$, $He^{2+}$, $Li^{3+}$ and $C^{6+}$ ions in liquid water. Values are calculated with the CDW-EIS formalism for the ionisation channel and with the Dingfelder *et al* (2000) model for the excitation channel. The recommendations of ICRU (ICRU 1993 and 2005) are also depicted. The overall accordance is good, with small discrepancies for the low-energy ions with increasing projectile charge because the ICRU data pertain to ions that are partially dressed at low energies.

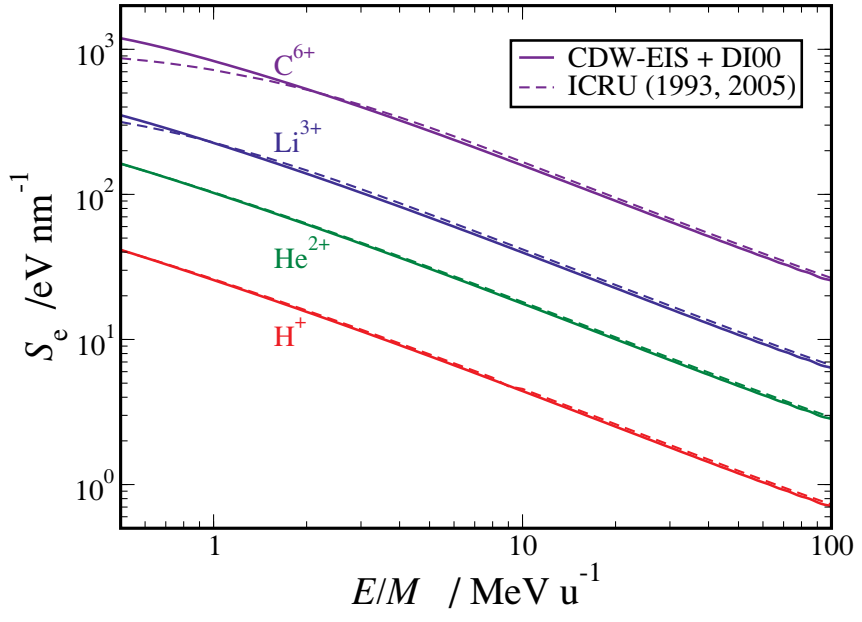


*Figure 3.2.* Electronic stopping power of $H^+$, $He^{2+}$, $Li^{3+}$ and $C^{6+}$ ions in liquid water as a function of energy. The continuous curves indicate total values obtained by summing the contributions from ionisation (CDW-EIS) and excitation (Dingfelder *et al* (2000)). The dashed curves are the recommendations of ICRU Reports 49 (ICRU 1993) and 73 (ICRU 2005).

### 3.1.2 Electrons

Electrons can mostly experience elastic, bremsstrahlung, excitation and ionisation interactions during their slowing down in liquid water.

**Elastic scattering**

Elastic scattering is not a mechanism for energy loss. Nevertheless, it induces relatively large angular deflections along the electron track, which results in very tortuous electron paths and a consequent spread out of the EDs caused by the inelastic interactions.

The state-of-the-art calculation for elastic scattering of electrons in any material was presented by Salvat *et al* (2005) and is based on the relativistic (Dirac) partial-wave method. As a matter of fact, both ICRU (ICRU 2007) and NIST have adopted the values from such calculations. A database with TCSs and SDCSs derived from this model is included in the general-purpose MC code PENELOPE (Salvat *et al* 2008).

**Bremsstrahlung**

Bremsstrahlung is the emission of electromagnetic radiation (a photon) produced by accelerated charged particles that interact with either the nucleus or the atomic electrons. Bremsstrahlung contribution to the energy loss of electrons in liquid water is almost negligible for energies below a few hundred keV, but becomes an important energy-loss mechanism above several MeV.

The SDCS database for all elements presented by Seltzer and Berger (1985, 1986) represents currently the gold-standard for bremsstrahlung of electrons with energies in the range 1 keV to 10 GeV, and it is incorporated in PENELOPE. The additivity rule can be used to compute the SDCS for any compound, such as the water molecule.

**Ionisation, excitation and atomic relaxation**

Electron inelastic interactions in liquid water are conveniently described by models for the dielectric response function of this substance. Dingfelder *et al* (1998, 2008) presented a model for the dielectric function of liquid water which is based on the optical measurements by Heller *et al* (1974) and fulfills the Thomas–Reiche–Kuhn sum rule. Based on recent spectroscopy measurements of inelastic x-ray scattering by Hayashi and co-workers, Emfietzoglou *et al* (2005) proposed an improved model, which yields a broader Bethe ridge, in accord with those experiments. Both approaches account for excitation and ionisation of liquid water. When a vacancy is produced in the innermost molecular orbital (the oxygen K shell), the subsequent relaxation process yields an Auger electron (or a characteristic x-ray, although this is much less probable) that can deposit energy far away from the ionised molecule. The ionisation of the inner shell is better represented by CSs computed within the relativistic distorted-wave Born approximation, thus including exchange and

distortion effects (Bote and Salvat 2008). Such a CS database is included in PENELOPE-2008. However, in track-structure codes the ionisation of the inner shell should be correlated to the energy lost by the projectile in order to preserve local energy conservation, which is not the case in standard PENELOPE. Indeed, the inelastic collisions of electrons in liquid water are described in PENELOPE with a generalized oscillator strength model with three discrete resonance levels for the excitation spectrum of the medium. Consequently, the spectrum of the kinetic energies of the ejected electrons is somewhat unrealistic and can distorsionate the spatial distribution of the EDs at the nanometre scale (cf. paper II). The (continuous) excitation spectrum of the medium is better followed by sampling the energy of the ejected electrons from a SDCS database calculated with the model by Dingfelder *et al* (1998, 2008). The model by Dingfelder *et al* (1998, 2008) has been recently updated (Dingfelder 2013) to include new available experimental data. Modifications to this model are not incorporated in this work.

### 3.1.3 Photons

The dominant interactions of photons with energies between 50 eV and 100 MeV are photoelectric effect, Rayleigh scattering, Compton effect, electron-positron pair production and photonuclear interactions when passing through matter. Only a deflection of the photon trajectory occurs in Rayleigh scattering, while the other interaction mechanisms also account for the EDs in the medium. These are well-known effects and of straightforward implementation in MC codes for radiation transport. See Salvat *et al* (2008) and references therein for a detailed description of the physics.

## 3.2 Track-segment conditions and particle transport

Some microdosimetric problems deal with the characterization and understanding of certain radiation properties for a fixed energy of the primary projectile, i.e. a small segment of the particle track. The average energy transferred from a light ion to a secondary electron in each ionisation is small. When the total simulated distance travelled by the primary particle is kept short enough so that the total energy lost is only a small fraction of the initial energy, the simulation resembles the so-called track-segment conditions. The length of the simulated track should be such that longitudinal equilibrium of the fluence of secondary electrons in the volume of interest is established. In these cases, for the sake of simplicity, two approaches can be applied to determine the energy loss of the primaries. The first method, continuous-slowing-down approximation (CSDA) (Qiang and Zengquan 1997), assumes that the projectile looses its energy gradually at a constant rate dictated by the stopping power. The second, which we call pseudo-transport simulation scheme

(paper I), keeps the DDCS distribution constant. We substract the energy lost by the projectile in each interaction but sample from a fixed DDCS distribution, i.e. for the same ion energy. Notice that pseudo-transport generates a more realistic ED pattern than the CSDA approach.

However, track-segment conditions might not be fullfilled for other microdosimetric studies, such as e.g. when the ED patterns from low-energy particles ($\sim$ 1 MeV/u) traversing a cell-nucleus-sized target of typical dimensions around 10 $\mu$m should be simulated in detail. Consequently, full transport simulation should be performed. Unfortunately, full transport requires longer simulation times than track-segment conditions due to the large amount of interactions that the particle experiences during the slowing down. The DDCS in the full-transport framework should vary with the projectile energy. On-the-fly calculation of the DDCSs with state-of-the-art models is not practical; databases for various projectile energies should be precalculated and stored. To account for changes in the projectile energy, we sample the DDCS table in the corresponding energy interval, from which angle and energy of the ejected electron are in turn sampled. This approach generates a realistic description of the energy loss of the primary particle and is faster but equivalent to linearly interpolate the DDCS in a dense grid (Benedito *et al* 2001).

## 3.3 LIonTrack: a track-structure MC code

We have developed a new MC tool for the generation of ED patterns by protons and other light ions with accuracy at the nanometre scale. The medium of interaction is liquid water. The MC code consists of two separate packages. Each package is structured so that the user can decide from the available scattering models which to apply. The HKS or CDW-EIS models can be selected for the transport of protons with energies in the 1–20 MeV/u interval. Only the CDW-EIS database is available for larger energies (1–300 MeV/u) or heavier particles ($Z \leq 10$). The excitation SDCSs are those from Dingfelder *et al* (2000) due to lack of reasonable alternative models. The first generation of electrons emitted from the impact of ions is thereafter transported and followed down to an absorption energy of 50 eV. Below such cutoff the remaining energy is deposited on the spot. The scattering of electrons can be simulated with the inelastic model (ionisation) included by default in the standard PENELOPE for arbitrary materials where accuracy at the nanometre scale is not necessary. Eventually, the user should activate (from the input file) the Dingfelder *et al* (1998, 2008) model for the inelastic (ionisations, excitation and relaxation) scattering of electrons in the bodies filled with liquid water where e.g. track-structure studies will be carried out. Figure 3.4 illustrates proton and carbon ion tracks simulated with the LIonTrack code. The higher ionization density for carbon ions than for protons along the track core is clearly manifested.

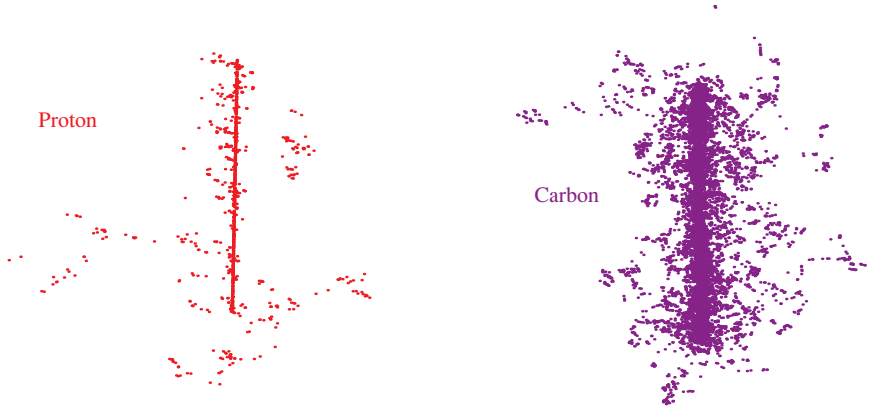


*Figure 3.3.* Proton (left) and carbon (right) ion track segments of 1 $\mu$m length for 1 MeV/u particles.

Photon radiation can also be simulated with the modified PENELOPE-2008. The interaction processes mentioned above are included therein, and the ejected electrons can be transported with either the default models or the Dingfelder *et al* (1998, 2008) inelastic SDCSs.

# 4. Frameworks to generate and investigate EDs at the subcellular level

A database of EDs generated by proton, helium, lithium and carbon ions of various energies was created to facilitate the investigation of ED structures. We focused on the study of EDs confined in volumes with the dimensions of cell nuclei, that for typical mammallian cells vary between 2 and 15 $\mu$m. A large number of EDs, on the order of $10^5 - 10^6$, occur in the target volume for typical absorbed doses of about 2 Gy. Figure 4.1 exemplifies the spatial structure of EDs in an 8 $\mu m^3$ volume irradiated by $^{60}$Co photons and 1 MeV/u protons.

We chose to emulate irradiation conditions similar to those in radiobiological experiments, through which RBE at different endpoints are established. Specifically, conservation of the secondary electron fluence in the target was sought. The shapes of the cell nuclei were approximated by cubes.

The methodology to resemble the generation of the EDs by photon and light ion irradiation of a cell nucleus-sized target for a given absorbed dose (cf. paper IV) is described in section 4.1. The cluster concept selected in this work to analyse the spatial patterns of EDs is defined in section 4.2 together with the method to score the ED clusters.

## 4.1 Generation of EDs

### 4.1.1 EDs by $^{60}$Co photons

$^{60}$Co photons are the common reference radiation used to determine the RBE of different radiation qualities. Hence, the EDs patterns by $^{60}$Co photons should be simulated in conditions equivalent to those for light ions. A straightforward methodology would be to place a cubic target (with cell nucleus dimensions) at 5 cm depth in a liquid water phantom, and simulate the irradiation by a $^{60}$Co point source located outside the phantom. However, event-by-event simulation of the secondary electrons ejected by the photons for an absorbed dose of 2 Gy in the target would require more than one year of CPU-time. A novel approach that takes advantage of the highly stochastic character of photon irradiation was designed to overcome this unviable computation. The method consists of two steps (see figure 4.2). First, a certain number of histories is simulated to yield EDs for a low absorbed dose in a volume much

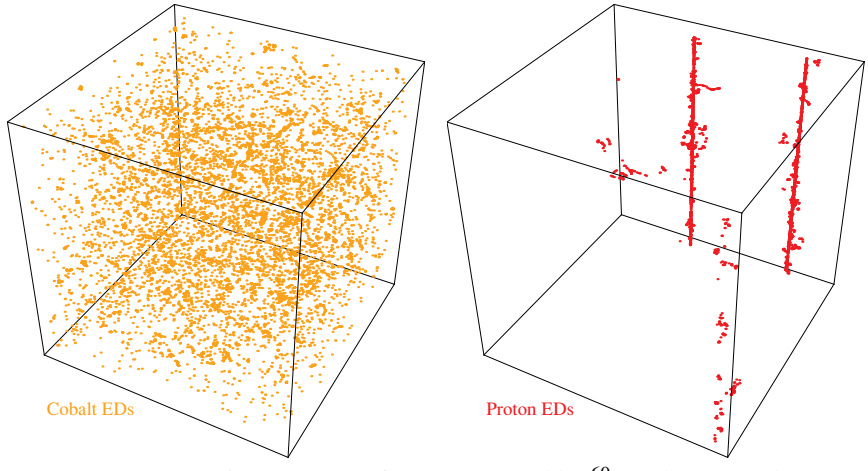


*Figure 4.1.* Representatitve patterns of EDs generated by $^{60}$Co photons and 1 MeV/u protons for an absorbed dose of 2 Gy in a cubic volume of $2\times2\times2$ $\mu$m$^3$. The total number of EDs is approximately the same, but they are more homogeneously distributed for the sparse radiation (i.e. $^{60}$ Co photons) than for the more densily ionising radiation (i.e. 1 MeV/u protons).

larger than the target. Second, the scoring volume is divided in cubes of dimensions equal to the target, select (discriminate) a number of these cubes, and assemble the EDs therein (by translating their positions) into one target volume (discriminating assembly-method).

The simulation time was also reduced by dividing the phantom in three regions with different simulation parameters for electron transport (see figure 4.2). In the innermost (scoring) body, centered at 5 cm depth, particle transport was simulated in an event-by-event mode. A concentrical shell around the scoring volume also with event-by-event simulation ensured conditions of charged particle equilibrium (CPE) in the scoring volume. In the outer region of the phantom only mixed simulation was required. The size of the scoring volume (about a couple of cm in length and one mm in depth) was chosen to be the largest possible and such that macroscopic variations of the dose homogeneity were less than 1% [1].

Two arrangements for the positive discrimination of $N_c$ cubes (enough to achieve a certain dose in the target) were tested. One arrangement selected equally spread out layers in depth ($z$) and thereafter equidistant cubes along the $x$- and $y$-axes [equidistant box selection (EBS)]. The separation between cubes was maximized for each dose level. The $N_c$ boxes in the other arrangement were randomly sampled along the three axes [random box selection (RBS)].

[1]We thank Dr. Karin Eklund for calculating dose profiles and dose depth curves to determine the optimal dimensions of the scoring volume.

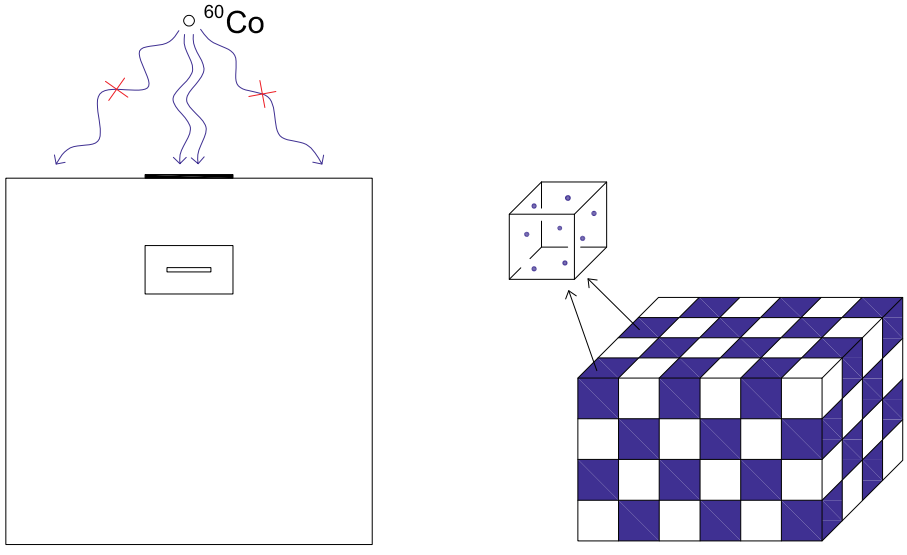


*Figure 4.2.* Sketch of the computational steps in the discriminating assembly method. The geometry setup to simulate and score the EDs generated by a $^{60}$Co source is delineated in the left picture. The liquid water phantom is divided into three regions with different simulation modes (mixed scheme in the outermost layer and detailed simulation in the inner regions). EDs are scored in the innermost volume. The picture to the right sketches the process to assemble EDs up to a given dose into a cell nucleus-sized volume. The innermost region of the phantom is divided into cell nucleus-sized volumes and some of those are positively discriminated (selected), i.e. the positions of their confined EDs are translated into one volume so as to achieve a certain dose level therein.

The simulation time was reduced to about a couple of days. The discriminating assembly-method execution times varied with the dose in the target and with the arrangement, being shortest for the EBS.

The suitability of the above method to generate EDs in the target by photon irradiation was analysed in various ways. The frequency distribution of distances to neighbouring EDs were calculated with both the EBS and the RBS. Figure 4.3 displays the frequency distributions, per imparted energy, of distances to the first ED neighbour at three dose levels (0.1, 1 and 10 Gy) for a cubic 10 $\mu$m side target. The curves calculated with the EBS and RBS arrangements of boxes overlap each other along the whole distance range, which indicates that the assembly method does not bias the spatial pattern of EDs. Additionally, the frequency distributions of ED distances were computed with the EBS for different gaps between the boxes, yielding identical results within

the noise levels. Again, the distributions were almost identical. The aforementioned tests yield the same results for a smaller cell nucleus with sidelength 2.5 $\mu$m.

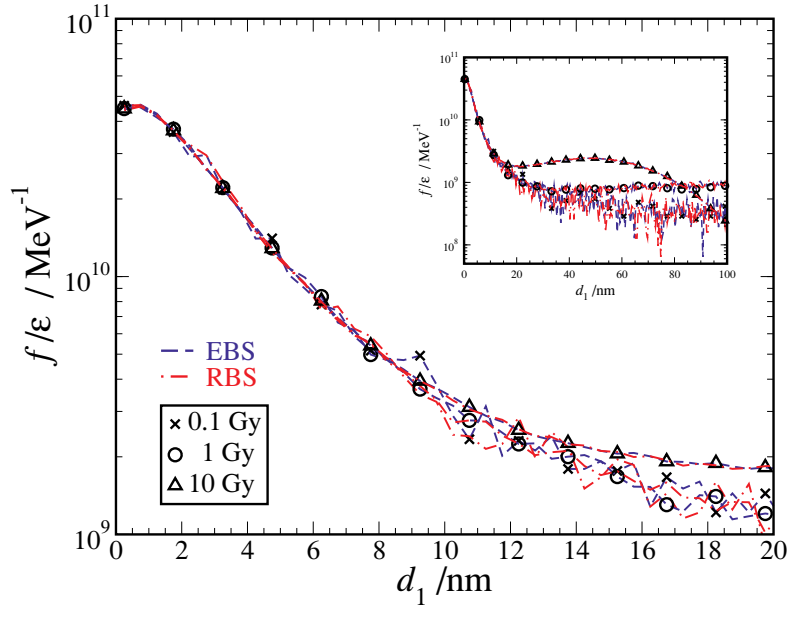


*Figure 4.3.* Frequency distribution of ED distances to the first neighbouring ED for $^{60}$Co photons in liquid water. Data calculated with the assembly discriminating method are displayed for the two arrangements of selected boxes, equidistant boxes (dashed lines) and random boxes sampling (dotted-dashed curves). The average absorbed doses in the cell nucleus (a cube of 10 $\mu$m side) are 0.1 (crosses), 1 (circles) and 10 Gy (triangles). The inset depicts the frequency distribution at larger distances.

### 4.1.2 EDs by protons and other light ions

The examined energies were mainly those in the Bragg peak (below about 60 MeV/u), because ions at such energies contribute the most to the energy deposition in the tumour, and are therefore of interest for the target dose optimization. The higher the particle energies, the more similar the ED patterns will be to those for the reference radiation.

Five hundred charged particle tracks for each selected nominal energy of the projectile were simulated. The initial energies were set to values such that the projectiles had slowed down to their nominal energies at the target centre. The lengths of the simulated tracks were equal to the target side plus a distance $d_{\mathrm{eq}}$ twice the CSDA range of the most energetic secondary electron that could be emitted. The irradiated area was a circle covering both the target surface and $d_{\mathrm{eq}}$ (see figure 4.4). These settings ensured conservation of the secondary

electron fluence in the target volume. The mean number of tracks $N_t$ to deliver the desired dose in the irradiated volume was calculated from the stopping power. The actual number of tracks was sampled from a Poisson distribution with mean value $N_t$. The positions of the tracks were randomly sampled within the circle. Finally, the distances from each ED within the target to its $M$ closest EDs were calculated.

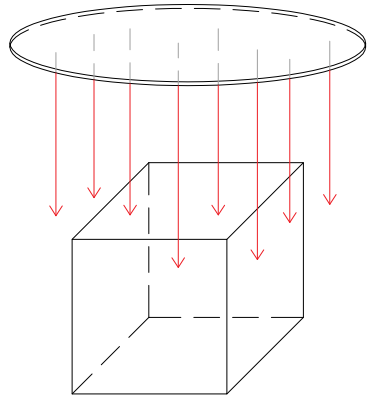

*Figure 4.4.* Schematic representation of irradiation of a cell nucleus-sized target. Arrows symbolize the ion tracks from the beam.

## 4.2 Cluster method

### 4.2.1 Cluster concepts

The definition of ED clusters (groups of EDs and related estimates of initial yields of DNA damage) proposed to date can be split in two groups. In one group the cluster scoring targets consists of water cylinders or spheres of a few nanometres (often two to ten) (see e.g. Charlton *et al* 1985, Nikjoo *et al* 1994), randomly placed in a larger volume of about the cell/cell nucleus size or sampled along the tracks. This type of method adds an artificial 'wall' to both the size of the cluster and where it is located, see figure 4.5, imposing an implicit assumption that a large continuous region of tightly located EDs outside the target cause no extra damage to what is caused by the EDs in the target. In the other group sophisticated and detailed DNA structures are superimposed to cell nucleus-sized volumes (see e.g. Ottolenghi *et al* 1997, Friedland *et al* 2005). These can be useful for explaining DNA damage mechanisms in detail, but are unlikely, due to their inherent complexity, to be practical for quantitative semi-mechanistic modelling of RBE data in clinical contexts.

The cluster method chosen in this work examines all EDs within a cell nucleus-sized volume. Cluster members are selected by a single criterion, be-

ing the maximum allowed distance to the closest neighbour in the cluster. This minimizes the assumptions and number of parameters in the analysis of radiation cluster patterns. Hence, a cluster is defined as a group of EDs such that each ED has at least one other ED within the clustering distance ($d_c$). Consequently, all EDs excluded from a cluster have a distance exceeding $d_c$ to all EDs in that cluster. This cluster concept implies that no specific ED (or position) within the potential cluster has priority over one another, whereas in approaches with cylinders or spheres a given *ad hoc* position (often one ED) determines the cluster geometrical centre. Figure 4.5 shows the different clusters that would be computed with the spherical and with the ED-ED distance cluster (used in this work) concepts for an hypothetical distribution of EDs. This situation illustrates how a large complex cluster of EDs according to the ED-ED distance algorithm is broken into several low order clusters with the spherical cluster method.

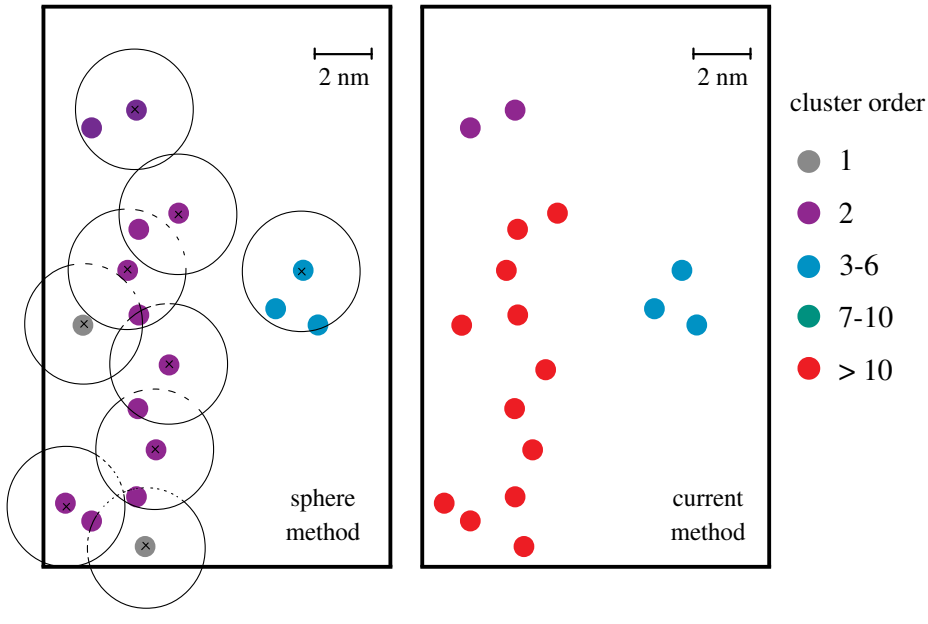


*Figure 4.5.* Illustration of the ED clusters computed by two different cluster methods for the same spatial distribution of EDs. This example assumes a clustering distance of 2 nm for both cases. The method in the left panel would compute as a cluster all EDs within a sphere with radius equal to the clustering distance and centered at a selected position (the first non-scored ED along the track). The clusters that would be computed with the current method are presented in the right panel, where all EDs that have one other ED within the clustering distance will belong to the same cluster.

Our approach quantifies the clusters of EDs by radiation in a more realistic way, but the correlation to a radiobiological endpoint might not be straightforward. For instance, it depends on the exact DNA distribution, which varies

with the cell cycle phase, and might also differ for normal and cancer cells. There might also be an energy threshold for an ED to cause DNA damage. These and other hypothesis might have to be considered in the specific frame of RBE modelling.

### 4.2.2 Cluster scoring algorithm

The input data needed by the clustering algorithm are (pre-computed) interdistances and indexes to the $M$ nearest EDs for each ED within the cell nucleus-sized target, where $M$ is large enough to include all presumptive cluster members. To find the $M$ nearest EDs to one ED requires to calculate the distance to all other EDs, and hence the time computation depended on the total number of EDs. This number varies with volume size and dose level, and for the present conditions was often too large to proceed with a serial calculation. The algorithm was parallelised (with OpenMP directives) to reduce the computation time.

Once the distances are available and a cluster distance $d_c$ selected, the algorithm proceeds as follows:

- appoint an ED not yet scrutinized to be the first member of a new cluster
- determine which of the $M$ closest EDs to the first member are within $d_c$
  - if none, close the cluster at order one
  - otherwise, add these EDs to the cluster
- neighbour search all new members in an iterative process until no more EDs join the cluster

The members of a cluster were excluded from the computation of other clusters, with aid of proper labeling. The indexes of the cluster members were recorded to facilitate post-analysis of various cluster properties.

The algorithm requires a sufficient scored number of neighbours, i.e. $M$ large enough so that all EDs within $d_c$ were listed. The sufficient number of neighbours increase with $d_c$, dose, and atomic number of the ion. $M = 98$ was adequate for low-energy protons up to 5 MeV/u with $d_c = 15$ nm, and up to higher energies for smaller values of $d_c$. However, larger values of $M$ are needed to compute ED clusters with a $d_c = 10$ nm for densely ionising radiation qualities such as e.g. 5 MeV/u carbon ions.

# 5. Particle track analysis at the nanometre scale

This chapter summarizes the main results of an extensive analysis of the EDs generated by $^{60}$Co photons and proton, helium, lithium and carbon ions and their secondary electrons in liquid water. The patterns of cluster formation of EDs were the primary object of study. Section 5.1 outlines the main features of the secondary electrons emitted by 1–20 MeV/u protons as simulated with the HKS DDCS and the default interaction models in PENELOPE. Section 5.2 covers the analysis of single ion tracks and (multi-track) irradiation of cell nucleus-sized targets at clinical dose levels. These results stem from simulation with the CDW-EIS and Dingfelder *et al* (1998, 2008) models in LIonTrack, except when otherwise stated.

## 5.1 Secondary electrons: slowing-down spectra

A large part of the energy deposition along an ion track occurs via secondary electrons, and their properties are therefore of prime interest. Thus, many studies have been undertaken regarding the slowing-down spectra of secondary electrons produced by different radiation qualities, their energy imparted spectra and radial dose distributions (Chen *et al* 1994, Cucinotta *et al* 1998, Uehara *et al* 2001, Uehara and Nikjoo 2002, Tilly *et al* 2002, Emfietzoglou *et al* 2004, Champion *et al* 2005, Nikjoo *et al* 2006). Investigations aided by MC codes provide the most detailed data. The availability of new CS data sets implemented in MC codes permits analysing the influence of the CS models on specific applications. For instance, the number of secondary electrons of high energies might be overestimated by certain models such as Rudd in detriment of the low-energy electrons, as revealed in figure 5.1. The low-energy electrons travel short distances before loosing their energy and, consequently, they originate EDs that are localized in the vicinity of the ion track. A larger number of EDs close to each other implies a higher frequency of complex ED clusters.

The better knowledge on the angular distribution of the emitted secondaries by particle impact might generate more accurate spatial patterns of EDs, that are examined in the following section.

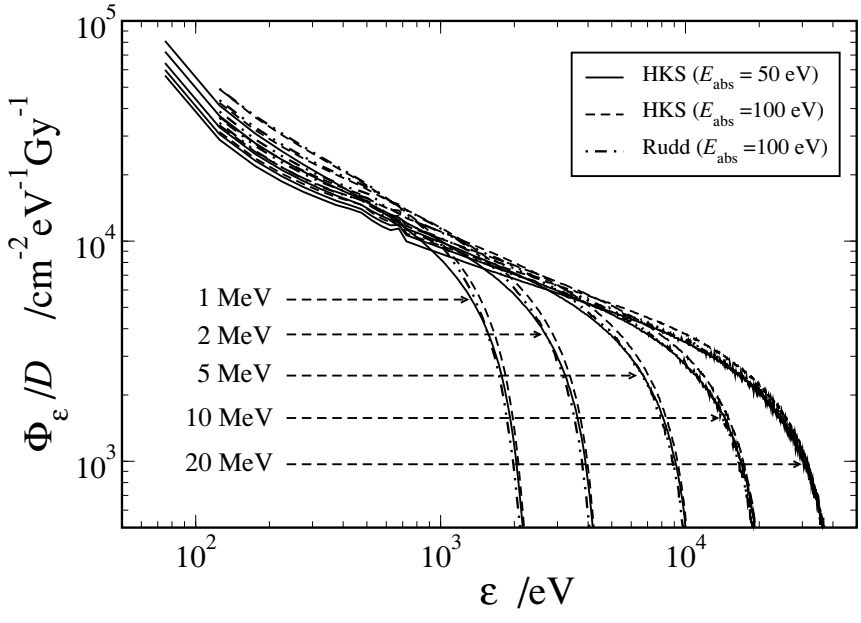


*Figure 5.1.* Electron slowing-down spectra in liquid water, generated by 1, 2, 5, 10 and 20 MeV protons. Spectra calculated with HKS DDCSs and $E_{\text{abs}}$ equal to 50 or 100 eV are plotted as solid and dashed curves, respectively, whereas the dot-dashed curves correspond to the results obtained by Tilly *et al* (2002) using Rudd's model and $E_{\text{abs}} = 100$ eV.

## 5.2 Light ions and $^{60}$Co-photons: Spatial patterns of EDs

A simple examination of the spatial distribution of EDs is to calculate the distance distribution for different orders of nearest neighbours. Such distributions are not biased by any *ad hoc* parameter, or assumption, and their behaviour can give some insights to clustering (see section 5.2.1). A certain overlap between particle tracks might occur for cell-nuclei-sized targets for certain absorbed dose levels and projectile energy, and thus modify the relative spatial distribution of EDs. Consequently, distance distributions for cell nuclei might differ from the distributions for single tracks. In contrast to nearest neigbhour distance distribution, the study of ED cluster formation requires an *ad hoc* parameter, as described in chapter 4.

### 5.2.1 Distances between EDs for single particle tracks

We quantified the relative contribution of primaries and secondaries to the closest ED distances for various proton energies (paper I). The number of closest pairs of EDs by the protons with higher LET mainly stems from the

protons themselves, i.e. in the track core, and constitutes approximately 55% of the total ED yield (table 2, paper I). Hence, track structure studies on RBE should carefully simulate the interactions of both the projectile and its secondaries, as the EDs caused by the light ion are a large contribution to the total.

Pairs of EDs with interdistance 2–3 nm for protons of 1 MeV/u were 5 times more frequent than for 20 MeV/u protons, which have a lower RBE (figure 5.2). On the other hand, 1 MeV/u carbon ions potentially generates at least 15 times more clusters of order six than 1 MeV/u protons for a $d_c$= 3 nm (figure 5.3).

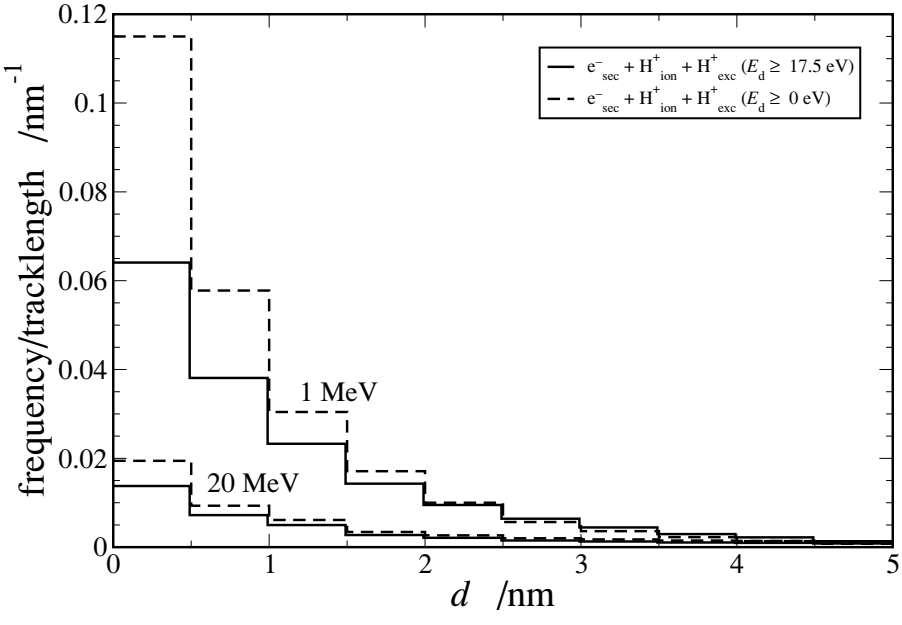


*Figure 5.2.* Frequency distributions of nearest-neighbour ED distances for 1 and 20 MeV/u protons in liquid water (normalized per track and length). Distributions were calculated with HKS DDCSs. Data are represented for only energetically-significant events, i.e. EDs larger than 17.5 eV (full curves and histograms), and for all events (dashed curves and histograms).

The frequency distributions of ED distances to the first and the fifth nearest ED crosses at larger distances with increasing atomic number of the projectile, due to the increasing ionising density (see e.g. figure 5.3). A larger crossing distance permits a higher formation of complex clusters of EDs.

We have calculated mean distances between various neighbour order EDs for light ions with specific energies 1, 5, 20 and 50 MeV/u. We concluded that the mean distances increase with neighbour order and particle energy, and decrease with the atomic number of the projectile (see table I in paper III for data).

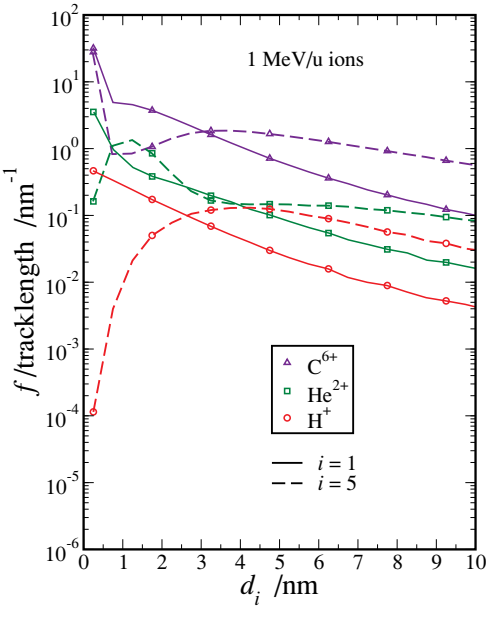


*Figure 5.3.* Frequency distributions of ED distances $d_i$, with $i$ equal to the first (continuous lines) and the fifth (dashed lines) nearest ED generated by 1 MeV/u light ions (normalized per track and length). Data correspond to protons (circles), helium (squares) and carbon ions (triangles).

The different physics models incorporated in the MC codes have an impact on the spatial patterns of EDs. The distributions of distances to the first ED are quite similar for both the CDW-EIS and the HKS models describing the ionisation of electrons by protons. However, the default models in PENELOPE causes the distributions of distances to decrease much faster with distance than for distributions with the Dingfelder *et al* (1998, 2008) model. This could yield a much smaller number of high order clusters of EDs, and consequently a larger number of ED clusters of low order.

## 5.2.2 ED clustering

**Frequency distribution of distances between neighbouring EDs**

The frequency distributions of distances to the first and the fifth neighbours are displayed in figure 5.4 (cf. figure 4, paper IV) for protons of 5 and 20 MeV/u traversing a cubic cell nucleus of 10 $\mu$m side. The mean absorbed dose to the target is approximately 2 Gy. The distributions presented in the previous sections were normalised per tracklength because scoring was restricted to a single track segment with lateral equilibrium of the secondaries, which length increased with particle energy. The current distributions pertain to volumes receiving different doses and therefore are normalised to the energy imparted

in the target. The frequencies of distances to the first neighbour are larger for the lower proton energy but decrease faster with distance for the lower energy. The curves for the first neighbour cross at approximately seven nanometres, where the frequencies for the longer distances become larger for the higher proton energy. Secondary electrons can have larger energies for higher energies of the projectile and, consequently, the distances between EDs are larger at the beginning of the electron tracks. The formation of ED clusters of order equal or higher than two will increase with a higher frequency of low distances to the first ED. Therefore, 20 MeV/u protons will yield a lower number of complex clusters than 1 MeV/u protons.

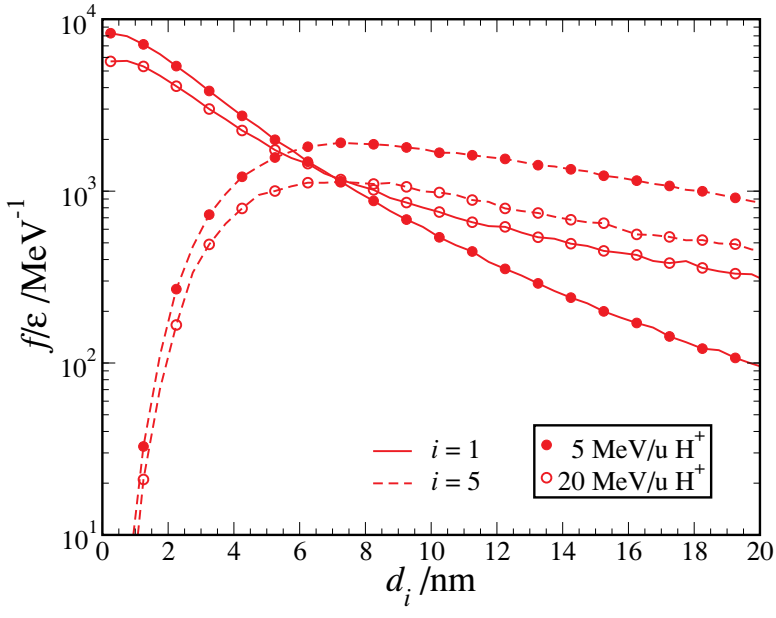


*Figure 5.4.* Frequency distribution per imparted energy of distances to the first (solid lines) and fifth (dashed curves) ED neighbours. The cubic targets of 10 $\mu$m side were traversed by 1 MeV/u (solid circles) and 20 MeV/u protons (empty circles) for absorbed doses of approximately 2 Gy.

**Frequency distributions of ED clusters**

The variations of the frequency distributions of ED clusters with radiation quality were studied in paper IV. Figure 5.5 displays results for $^{60}$Co photons and only 1 MeV/u particles.

The frequencies of ED clusters by $^{60}$Co photons were higher than the other radiation qualities for small cluster orders (1–2), but decrease steeper than the other light ions. This is in accordance with experimental results that reveal a higher formation of small fragments of DNA for ion irradiation as compared to photons (Stenerlöw *et al* 2002). The smaller fragments are associated to

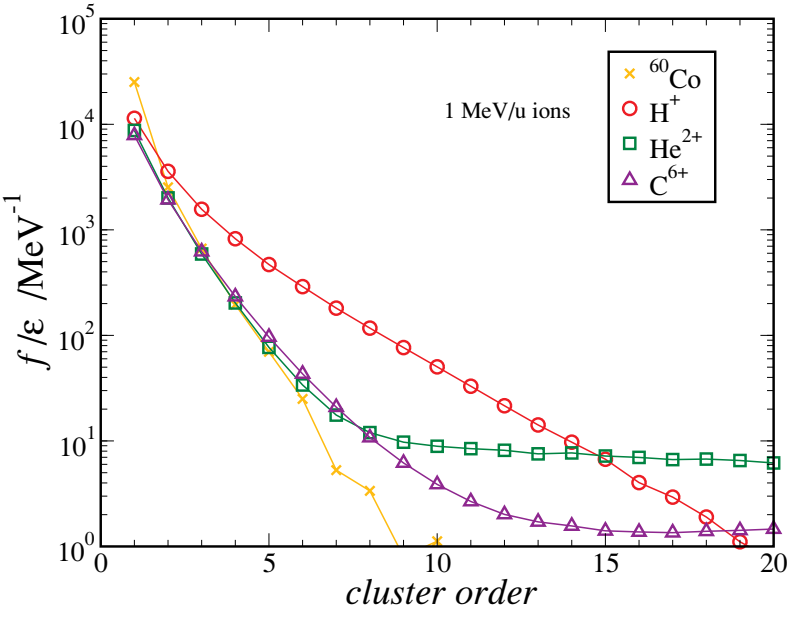


*Figure 5.5.* Frequency distributions per imparted energy of clusters of EDs for $^{60}$Co photons and proton (circle), helium (square), and carbon ions (triangle) of the same specific energy, 1 MeV/u.

multiple damage caused by many interactions breaking the DNA att many locations. The frequency distributions of ED clusters for 1 MeV/u carbon decreased faster with cluster order than for protons, and presented two regions. The higher frequency of cluster orders lower than 15 for protons than carbons is in accordance with the experimental RBE behaviour for low LETs below about 30 eV/nm, where protons have a higher RBE than carbon ions, and therefore a higher yield of complex ED clusters is to be expected. The high clusters orders are mainly formed in the vicinity of the track core, as can be seen in figure 5.6. Carbon ions of high LET (figure displays three radiation qualities in order of increasing LET) give rise to clusters of even higher order (see variation with the cluster order along the columns) than protons due to the higher ionising density of the carbons. The EDs by electrons contribute very little to the formation of complex clusters along their paths. However, the EDs along the track core are the main mechanism of formation of complex ED clusters.

The frequency distributions of ED clusters for different light ions with equal LET are displayed in figure 5.7. The frequency of cluster order one increased with atomic number of the particle, but the distributions cross between order two and three and thereafter decreased steeper with atomic number. This behaviour is in accordance with experimental measurements of the RBE that reveal lower RBE values for light ions with higher atomic number but equal

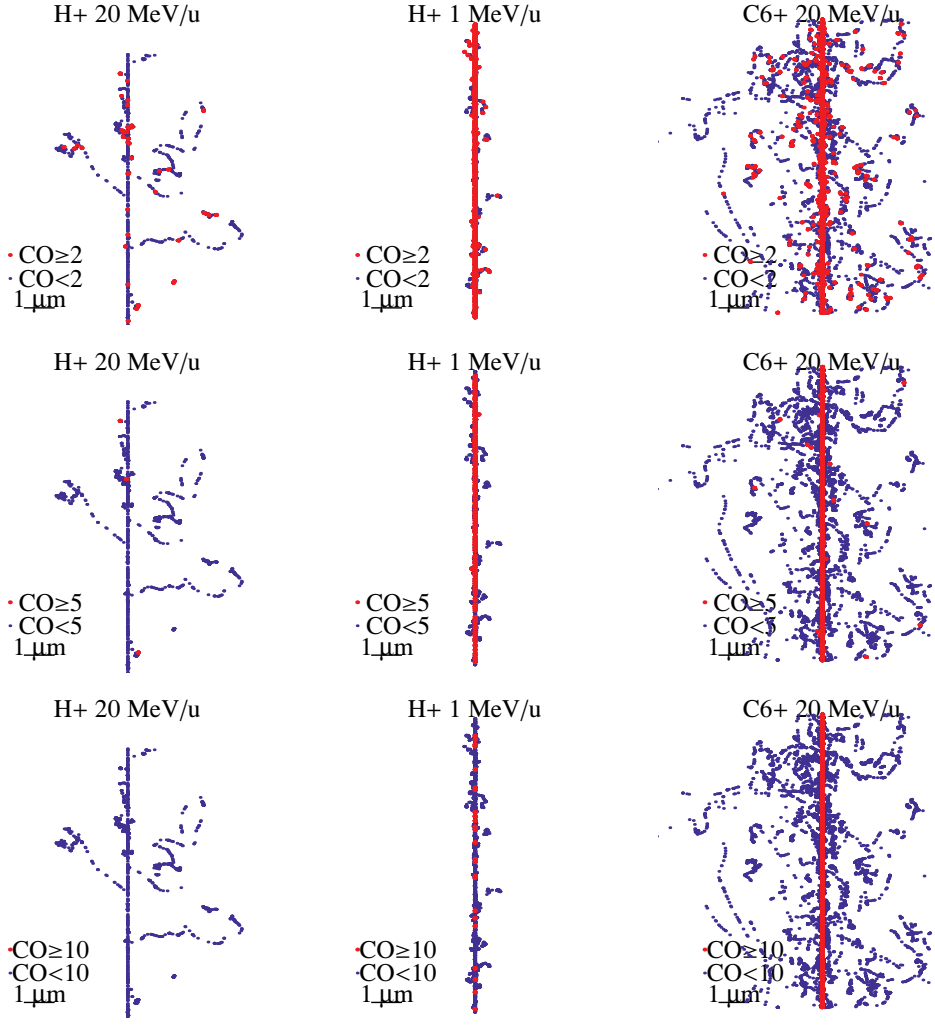


*Figure 5.6.* Diagram of ED clusters of low (blue) and high (red) order computed along particle tracks. The cutoff parameter for high order is set to two, five and ten (from top to bottom). First column are ED clusters for 20 MeV/u protons, second column correspond to 1 MeV/u protons, and the third column are data for 20 MeV/u carbon ions; i.e, panels from left to right are ED clusters formed by particles with increasing LET.

LET, in the region of LETs below approximately 30 eV/nm. This feature suggests that the distribution of frequency of clusters could be a good starting point for modelling of the RBE. However, the ED cluster distributions are sensitive to the value of $d_c$. The larger the $d_c$, the higher the number of ED clusters with high order and, consequently, the lower the number of clusters with few EDs due to conservation of the ED number in the target volume. The

precise value of $d_c$ has to be chosen within a specific radiobiological context, but can also be aided by knowledge on the general trends of ligh ion RBE. The distributions of ED clusters for various radiation qualities were computed for $d_c$ equal to 2 and 10 nm. We can conclude from figure 5.8 that the selection of $d_c = 2$ nm is a better choice when utilizing ED clusters for modelling of the RBE as the frequency of higher cluster orders follow the general trends of experimental RBE values.

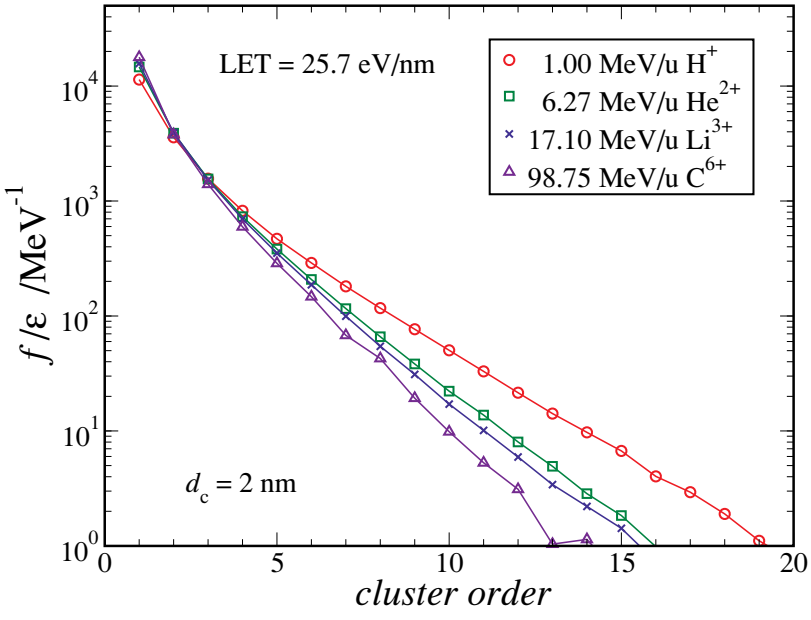


*Figure 5.7.* Frequency distributions per imparted energy of clusters of EDs for light ions with LET= 25.7 eV/nm. The specific energies of the particles are 1 MeV/u for the proton (circle), 6.27 MeV/u for the helium (square), 17.10 MeV/u for the lithium (cross) and 98.75 MeV/u for the carbon ion (triangle). The larger number of clusters of high order for protons as compared to the other ions correlates with the RBE.

**Properties of the clusters of EDs**

The absolute yield of clusters for the same radiation quality varies with target size and absorbed dose. Such variations can be handled by scaling, provided linearity within the range of interest. The frequency distributions of cluster orders were linear with dose in the clinical regime (e.g. 1–10 Gy) for cluster orders statistically significant. The distributions were also linear with target volume for most sizes of cell nuclei (2–15 $\mu$m) (paper IV). Departure from linearity should be expected for very large doses when secondary particle tracks start to overlap.

Energetical and geometrical properties of the clusters were investigated for various radiation qualities. Figure 5.9 depicts distributions of the total energy

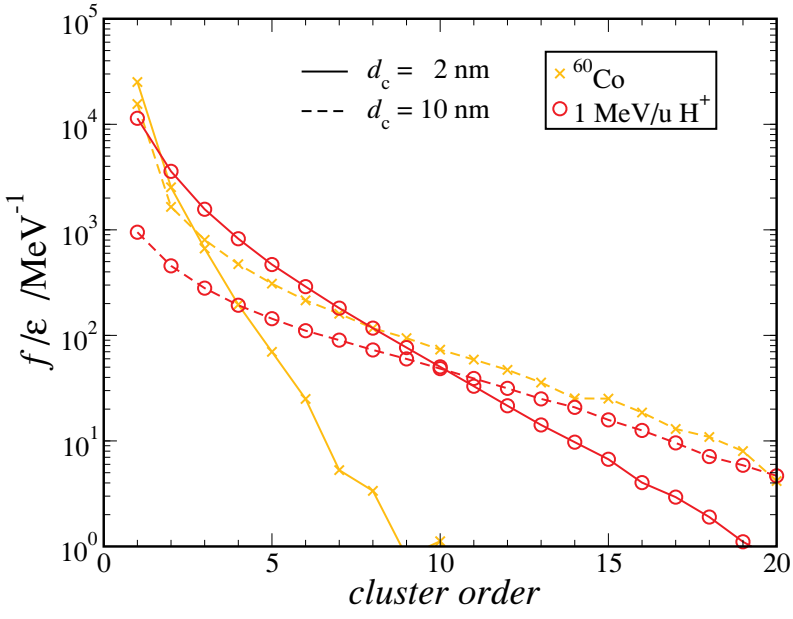


*Figure 5.8.* Frequency distributions per imparted energy of clusters of EDs computed with $d_c = 2$ nm (solid lines) and $d_c = 10$ nm (dashed curves) for the 1 MeV/u protons (circles) and $^{60}$Co photons (crosses).

in a cluster (energy sum of EDs in a cluster) as function of cluster order. The carbon ions (left panel) are more densely ionising and can yield more high order clusters than less dense ionising particles. There was a relatively large spread in energy for clusters of order less than 50; above that, the cluster energy tend to increase proportional with the cluster order. Protons mostly did not form clusters with such high orders. Different light ions with equal LET (right panel) had similar distributions, with somewhat higher cluster energies for the particles with lower atomic number because the number of higher cluster order was larger. The larger number of complex ED clusters for protons than heavier ions, at LET of 25.7 eV/nm, is in accord with the higher RBE of the protons (see comment in connection with figure 5.7).

The variation of the cluster radius (the distance from the mean position of the EDs to the most distant ED in the cluster) with cluster order for various radiation qualities is depicted in figure 5.10. The radius of the ED clusters increased with increasing number of EDs in the cluster. A linear increase in size with cluster order is only possible if the EDs are on a row. Clusters by carbon ions were often more larger than for proton ions, which is in accordance with the description presented in figures 5.5 and 5.6, i.e. large clusters occur within the track core and will most probably have long shapes. These clusters are probably very efficient in inactivating the cell as they can probably damage the DNA at multiple locations.

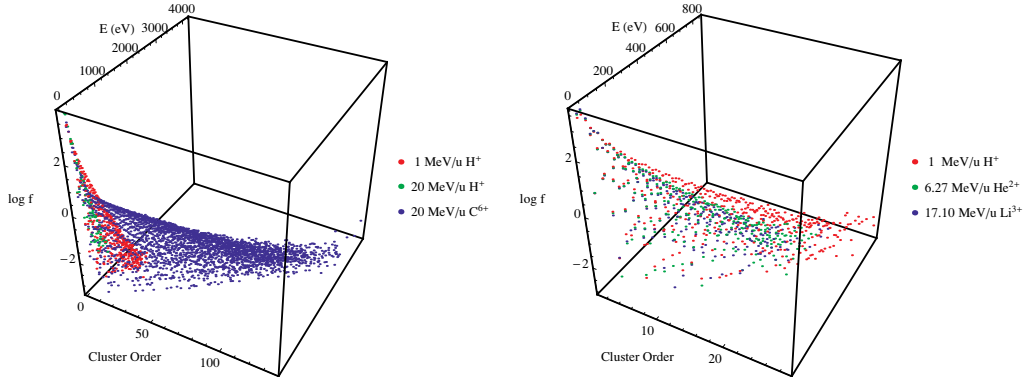


*Figure 5.9.* Frequency distributions of cluster energy differential in cluster order. The left panel are distributions for 1 MeV/u protons (red), 20 MeV/u protons (green) and 20 MeV/u carbon ions (blue). Frequencies in the right panel were obtained for light ions with LET=25.7 eV/nm. The specific energies of the particles are 1 MeV/u for the proton (red), 6.27 MeV/u for the helium (green) and 17.10 MeV/u for the lithium (blue).

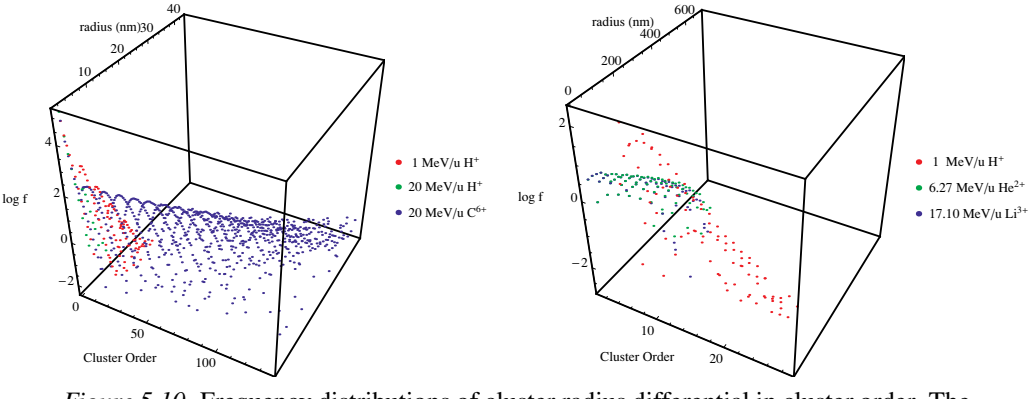


*Figure 5.10.* Frequency distributions of cluster radius differential in cluster order. The left panel are distributions for 1 MeV/u protons (red), 20 MeV/u protons (green) and 20 MeV/u carbon ions (blue). Frequencies in the right panel were obtained for light ions with LET=25.7 eV/nm. The specific energies of the particles are 1 MeV/u for the proton (red), 6.27 MeV/u for the helium (green) and 17.10 MeV/u for the lithium (blue).

# 6. RBE modelling based on ED clusters

Biological response data for photon treatments are often known from clinical data but less available for other radiation qualities. A reliable and robust modelling of RBE data could help in optimizing treatment strategies for numerous applications in radiooncology. This is, however, a challenging task due to the dependency of RBE on a number of variables (cell/tissue type, radiation quality, endpoint, etc.). Indeed, a consistent and sufficient experimental RBE data set does not exist (Holzscheiter *et al* 2012), neither from clinical trials or radiobiological experiments. Table 6.1 lists radiation qualities for which RBE has been measured for the same cell type (V79) and endpoint (cell survival), and that were determined experimentally in track segment conditions. We used these data for a preliminary investigation of RBE modelling.

Radiation response is commonly described by the the linear-quadratic (LQ) model which in its most basic form describes the survival curve, $S$, by an exponential curve of the form

$$S(D) = \exp(-\alpha D - \beta D^2), \tag{6.1}$$

where $D$ is the physical dose, $\alpha$ is determined from the slope of the curve and $\beta$ from the shoulder of the curve in a logarithmic scale. The cell survival is most often experimentally determined via clonogenic assays for various doses of exposure from which $\alpha$ and $\beta$ can be derived, but the LQ model is also used to parameterize clinical response data. Some interpretations of the LQ model associate $\alpha$ to the unrepaired damage, while $\beta$ is associated to the repair capacity of the cell (Sachs *et al* 1997).

A way to model RBE is to employ the LQ model but establish a formalism to predict the radiation quality dependent $\alpha$ and $\beta$ parameters. The induction of complex radiation clusters has been pointed out to be a major mechanism behind RBE variation (see e.g. Goodhead 2006, Schardt*et al* 2010). Hence, ED cluster data of the type presented in papers I,III–IV, are reasonable candidates to use for modelling of biological response parameters. The presence of high order ED clusters might be the base to create a surrogate of complex DNA damages, that are more difficult to repair, and therefore could potentially correlate to $\alpha$. Likewise, the low orders of ED clusters might represent the more repairable damage and hence be correlated to $\beta$.

We computed the frequencies of clusters orders of EDs for the radiation qualities in table 6.1 and $^{60}$Co photons in a liquid water cube of 12 $\mu$m side. The cube dimensions were chosen to match the average volume of the nucleus

**Table 6.1.** *$\alpha$ and $\beta$ parameters for published experimental data corresponding to 10% survival for the V79 cell line.*

| radiation quality | | $\alpha$ ($Gy^{-1}$) | $\beta$ ($Gy^{-2}$) | reference |
|---|---|---|---|---|
| | $E$ (MeV) | | | |
| $^{60}Co$ | 1.25 | 0.126 | 0.0345 | Stenerlöw *et al* 1995 |
| | $EM^{-1}$ (MeV $u^{-1}$) | | | |
| $H^+$ | | | | |
| | 0.91 | 0.74 | 0.011 | Folkard *et al* (1996) |
| | 1.40 | 0.469 | 0.043 | Belli *et al* (1998) |
| | 1.72 | 0.45 | 0.028 | Folkard *et al* (1996) |
| | 3.18 | 0.372 | 0.036 | Belli *et al* (1998) |
| | 3.59 | 0.32 | 0.039 | Folkard *et al* (1996) |
| | 4.97 | 0.0289 | 0.024 | Belli *et al* (1998) |
| $C^{6+}$ | | | | |
| | 4.06 | 0.639 | 0.0039 | Weyrather *et al* (1999) |
| | 5.27 | 0.99 | 0.022 | Weyrather *et al* (1999) |
| | 10.95 | 0.91 | 0.044 | Weyrather *et al* (1999) |
| | 76.70 | 0.337 | 0.025 | Weyrather *et al* (1999) |

of V79 hamster lung cells reported by Datta *et al* (1976). Two cluster distances were tested, $d_c = 2.0$ nm as it represents the distance between the backbones in the DNA, and $d_c = 3.4$ nm which is the distance between ten base pairs (a parameter generally assumed in estimations of dsb, see e.g. Nikjoo *et al* (1999). Furthermore, the frequency distributions of cluster orders were parameterized in terms of $d_c$ to enable data interpolation for any value of $d_c$ in the range 2.0–3.4 nm.

We studied first a proportionality relation between the reported $\alpha$ values and the ratio of the cumulative function of the frequency clusters of high order (frequencies below a certain cutoff not included) to the cumulative function of the frequency of all ED cluster orders. The cutoff order value was chosen to yield the best correlation to experimental data. This function described well $\alpha$ for protons, but did not fit the carbon data (results not displayed). The complexity of the ED clusters might be understood as a two-fold contribution, namely the cluster order and the proximity of the EDs in the cluster. The larger clusters occur mainly in the core track (as discussed in chapter 5) and therefore have often a more elongated shape. Long, elongated clusters may be more damaging than more curled clusters, and as long clusters mostly occur in the track core they may have a shorter nearest neighbor distance than curled clusters. Hence, a surrogate measure for complex damage $S_{CD}$ could be defined

as

$$S_{\mathrm{CD}} = \frac{\sum_{k}^{\infty} f_{d_c}(CO)\left(\frac{CO}{\bar{d}_1}\right)^2}{\sum_{1}^{\infty} f_{d_c}(CO)\left(\frac{CO}{\bar{d}_1}\right)^2}, \tag{6.2}$$

where $k$ is a cluster order cutoff value and together with $d_c$ are the free parameters of the model, $f(CO)$ is the frequency distributions of cluster orders, and $\bar{d}_1$ is the mean nearest neighbour distance. The quadratic term can be interpreted as a radiation quality dependent measure of the number of ED pairs with interdistance less than $\bar{d}_1$.

A preliminar analysis with yields of EDs cluster order estimated for the present data set gives the best fit ($r = 0.87$) for $k = 4$ and $d_c = 2.3$ nm, see figure 6.1.

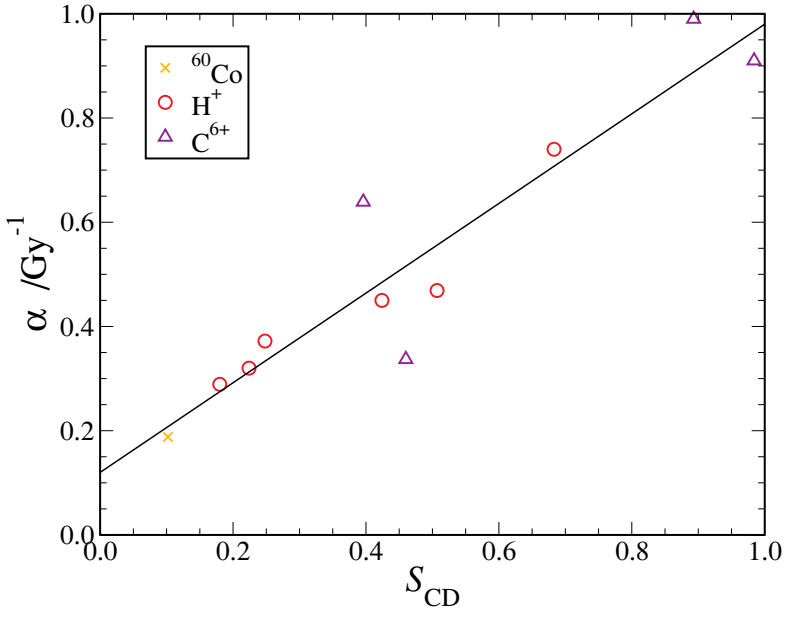


*Figure 6.1.* Experimental $\alpha$ corresponding to cell survival of V79 cell lines plotted as function of a surrogate measure of complex damage, $S_{\mathrm{CD}}$ for carbon ions (triangles), protons (circles) and $^{60}$Co photon (cross).

Likewise, an analogous surrogate measure for simple damage, $S_{\mathrm{SD}}$, can be defined as

$$S_{\mathrm{SD}} = \frac{\sum_{1}^{k-1} f_{d_c}(CO)\left(\frac{CO}{\bar{d}_1}\right)^2}{\sum_{1}^{\infty} f_{d_c}(CO)\left(\frac{CO}{\bar{d}_1}\right)^2}. \tag{6.3}$$

Unfortunately, experimental $\beta$ values present no clear trend when varying radiation qualities. This difficults the prediction of $\beta$ with any approach that employs experimental data. However, the results do not differ much from assuming a simply constant $\beta$, see figure 6.2.

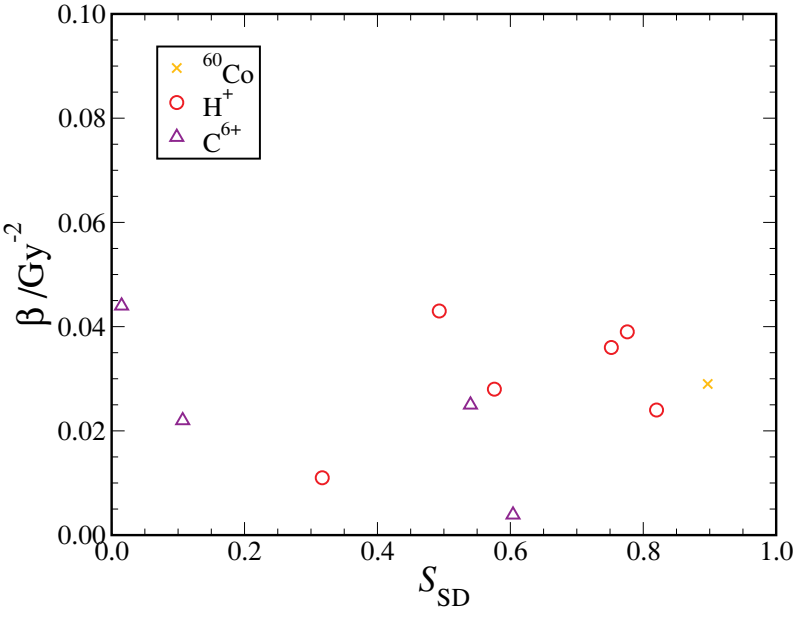


*Figure 6.2.* Experimental $\beta$ values as function of a surrogate measure of simple damage, $S_{\mathrm{SD}}$ for carbon ions (triangles), protons (circles) and $^{60}$Co photon (cross).

These preliminary results indicate that experimentally derived $\alpha$ values have a proportionality relationship to the frequencies of cluster orders, that can be explored in further modelling. If $\alpha$ for photons have any predictive power in this kind of semimechanistic model, as used e.g. in the LEM model (Friedrich *et al* 2012), remains to be tested.

# 7. Summary and Outlook

The main purpose of this thesis was to quantize the spatial patterns of EDs at the nanometre scale in irradiated liquid water for different radiation qualities. Such radiation quality specific data might prove useful to assess and understand the mechanisms behind RBE variations with radiation quality.

The spatial patterns of EDs were generated with MC codes. Various features of the electron EDs were studied with the aid of the PENELOPE package (paper I). The limitations of PENELOPE as a track-structure code were investigated and described in paper II. The main drawback was found to be the simplistic oscillator description of the inelastic scattering of electrons in liquid water. The electron inelastic model by Dingfelder *et al* (1998, 2008) was therefore coupled to the standard PENELOPE code as to enable accurate simulation of the spectrum of secondary electrons. This yielded a different spatial distribution of the EDs and, in particular, an increase of the frequency of distances to nearest neighbours for large neighbour distances as compared to the default models in PENELOPE. Furthermore, a MC tool, LIonTrack, suitable for track-structure simulations of light ions with energies in the range of 1–300 MeV/u was developed (paper III). The frameworks for generation and subsequent analysis of spatial ED patterns for different doses in targets with the size of a typical cell nucleus from irradiation were designed and validated, both for light ions and $^{60}$Co photons (paper IV). The latter radiation quality was studied as it is the common reference radiation applied in radiotherapy, and it is the common reference radiation use to determine RBE data. The methodology developed for $^{60}$Co photons can also be applied to study the spatial patterns of EDs for brachytherapy sources.

A clustering concept not biased by any specifically superposed scoring volume for characterization of the spatial pattern of radiation was introduced to quantify clusters of EDs. The objective differs from previous works in this field that focused more on scoring yields of DNA damages than in the radiation's properties. An extensive analysis of the spatial patterns of EDs for various radiation qualities with special focus on clustering features was carried out throughout this thesis. A first group of analysis quantified the partial contributions of the EDs by the protons themselves as compared to the secondary electrons for single particle tracks at low energies (paper I). This lead to the conclusion that track structure studies should include the EDs from the primary ion itself. Furthermore, the relative primary particle contribution to the yield of closest EDs was also scored for single proton tracks and other light ions. The EDs generated by the protons themselves contribute about

40% to the formation of pairs of EDs within the track for the lower proton energies. This contribution decreases with energy down to approximately 27% for 20 MeV/u protons. The mean distances between neighbours increase with particle energy (paper III). However, the increase was smaller for the projectiles with higher atomic number due to their higher ionisation density. The frequencies of ED clusters occurring in cell-nucleus-sized volumes have been computed for $^{60}$Co photons (as a reference radiation) and for proton, helium, lithium and carbon ions (paper IV). The yields of small cluster orders, e.g. one and two, were higher for the $^{60}$Co photons than for the light ions. The frequencies of ED clusters of order 2–15 were larger for the protons than for other light ions at the specific energy of 1 MeV/u. This is in good accordance with experimental data on RBE values for protons and light ions, under the assumption that the complexity of ED clusters correlates to the complexity of the DNA damage inflicted. The frequencies of high clusters orders were lower for protons with higher energies due to their lower ionisation density. The clusters were mostly formed by the EDs along the electron paths and therefore the clusters distributions were similar to those caused by the photon reference radiation. However, heavier light ions have a higher ionisation density than 1 MeV/u protons, and therefore yield more ED clusters of higher order. This is also in line with the general behaviour of experimental measurements of the RBE. The yields of ED clusters of order larger than three for particles with the same LET (see figure 5.7) decreased with increasing atomic number of the ion. This feature relates to the experimental lower RBE of ions with higher atomic number but same LET, encountered at low LET values. In conclusion, the RBE variations could be understood in terms of the distributions of frequencies of complex ED clusters, even for those radiation qualities that LET failes to explain. Therefore, frequency distributions of ED cluster orders were considered good candidates to define surrogate measures of radiation response substituing dose and LET as main predictors.

The possibility of modelling RBE as a function of clusters of EDs was preliminarly explored for experimental data on cell survival obtained under track segment conditions for the V79 cell line. A surrogate quantity for complex DNA damage function of the cluster order yields was defined and found to be linearly proportional to the $\alpha$ parameter of the LQ model. Hence, the frequency of ED cluster of different orders appears to be a suitable descriptor of the radiation quality that could aid to establish a surrogate for predicting $\alpha$. Future work should extend the analysis to alternative functions of the cluster order yields, to other cell lines and to more radiation qualities. Hopefully, the tools (MC codes, methodologies and analysis programs) developed in this thesis, and the acquired knowledge of the spatial characteristics of EDs for different radiation qualities can facilitate the future exploration of semi-mechanistic modelling of the RBE and, ultimately, contribute to the improvement of radiotherapy.

# 8. Sammanfattning på svenska

Vid strålterapi är målet att sterilisera cancercellerna genom att inducera strålskador på deras DNA samtidigt som man strävar efter att belasta omkringliggande friska vävnader med så låg stråldos som möjligt. En hjälp för att uppnå dessa motstridiga mål kan vara att optimera valet av strålning, dvs typ av partiklar och deras energi, utifrån deras specifika växelverkansmönster. Av speciellt intresse är den ökade förmågan att generera kluster av energideponerande (ED) joniseringar som jonstrålar med högre energiöverföringsförmåga (Liner Energy Transfer, LET) uppvisar, och som resulterar i olika relativ biologisk effektivitet (RBE). Komplexiteten av ED-kluster visar samband med komplexiteten till av strålningen orsakade DNA skador där man visat att komplexare skador är svårare för cellen att reparera och därför kan leda till att den inaktiveras. Det är därför av intresse att kartlägga förekomsten och komplexiteten hos energideponeringsklustren för olika strålslag, vilken skulle kunna ligga till grund för att hitta enkla mått baserat på klusterfördelningar till att förutsäga en given strålnings verkningsförmåga i termer av dess RBE värde.

I detta arbete har vi framställt energideponeringskluster och analyserat deras varierande komplexitet och mönster, på nanometernivå, för olika energier av protoner, helium-, litium- och kol-joner. En Monte Carlo kod, LIonTrack, dedicerad för spårstruktursimuleringar har utvecklats för att simulera lättjonspår i vatten (i vätskefas) med hög precision. Metoder för att beräkna EDs, för både $^{60}$Co fotoner och lätta joner, i strålmål av cellkärnestorlek för kliniska dosnivåer har tagits fram och använts för strålmål av vatten (i vätskefas). Alla dessa EDs har senare analyserats och kluster av EDs av olika ordningar har skapats. Detta skedde med hjälp av en av oss speciellt utvecklad klusteringsalgoritm som använder sig av en enda parameter, det maximala avståndet till närmaste ED.

Det direkta bidraget från jonerna själva till det totala antalet ED utgör upp till en 40% för 1 MeV/u protoner, och minskar med partikelns energi (paper I). Detta betyder att partiklarnas egna bidrag måste räknas in vid analyser av joniseringsmönster. Antal kluster av högre komplexitet (med 2–15 medlemmar i klustret) är större för 1 MeV/u protoner än för koljoner med samma energi (paper IV). Detta korrelerar bra med det faktum att protoner har en högre RBE värde för denna energi än koljoner. Olika joner med lika LET runt 25 eV/nm skapar också färre kluster av hög ordning för lättare joner, vilket stämmer med den beteende av RBE variationer som kan inte förklaras med LET. Antal komplexa kluster av hög komplexitet ökar med partikelns atomnummer för energier som också ger en högre RBE, som till exempel för 20 MeV/u kol i jämförelse med 1 eller 20 MeV/u protoner.

De verktyg och metoder som har utvecklats i denna avhandling kan underlätta sökandet efter en semimekanisk modell för RBE.

# 9. Acknowledgments

I have no words to express my truly gratitude to my supervisors Anders Ahnesjö, Nina Tilly and José M. Fernández-Varea for sharing with me their enthusiasm in this field and guiding me throrought this thesis. Specially thanks to Nina and Anders for the many enjoyable brainsstorming sessions and intensive discussions with always time for some touch of humour. Indeed, I admired your promptness to answer my questions any time, Anders, and I am happy for you pushing me to give my best even to the very last moment. Nina, you really encouraged me and enhanced my self-confidence through your positive criticism. José, thanks for the many didactic Skype discussions on radiation physics but in particular for opening me the door to the research world. Thanks to Bengt Glimelius for welcoming me as a member in the research group at the medical physics department.

Jag vill tacka mina vänner och gamla och nuvarande kollegor från Ackis för de trevliga stunderna tillsammans, både på jobbet och utanför. Jag kommer alltid att minnas bland annat de många skratt vi hade under 'svenskakursfikastunderna' med Karin och Calle i tidernas begynnelse. Karin, du hjälpte mig att få en annan perspektiv på allt möjligt, och du är en riktigt bra vän. Calle, det var roligt att resa med dig till alla kurserna, man blev aldrig utråkad. Kenneth, David, and Fernanda, it has been nice to share part of this journey with you.

Thanks to Anders M., Carina, Elisabeth, Christina V., and all others I have met in the Sjukhusfysikavdelningen for your warm welcome from the first day, and for the many laughs at 'Majsans fik' during these years. It was also kind of you to answer my questions about the clinical work, and to get me, and the other Ph.D. students, on board for the leasure activities.

I also get the pleasure to meet the other PENELOPE developers, Francesc Salvat and Josep Sempau, who shared their knowledge on radiation physics and Monte Carlo simulations with me.

And of course, my friends '*los peneloperos*', Ricardo, Vanessa, Javier, Imma and Andreu . . . I hope we now find some time to catch up.

I would like to send a hug to my catalan friends for being throughout, despite the distance. Cristina, you kept me company with your 'green ball' though there were times we were too busy to even say hello, you answered my crazy questions about fortran and linux, and you were the best link to Roser F., Roser C., Gerard, Alba, and Montse.

Thanks to my family for your thoughts on me. Specially to my mother who taught me that a dream is worth to fight for and also to be patience, two

essential ingredients in this thesis. Mil gracias mamá por enseñarme a luchar por mis sueños, a ser paciente y perserverante, y sobretodo por renunciar a mi compañía para que yo pueda ser plenamente feliz. Gracias a ti Laura, mi hermana pequeña, por tu fe en mí que ha sido fuente de aliento en muchos momentos. Tack också till mina svärföräldrar för ert stöd, så att jag kunde jobba extra när det behövdes och för att ni alltid ser till att vi kan ha det trevligt.

Men framförallt, tack till dig Pär, för att du älskar mig och igenom din kärlek har du stött mig. Du har accepterat med tålamod att jag '*bara*' skulle jobba '*lite till*'. Vi skrattar tillsammans, du skapar lugnt och ro hos mig, och du har uppmuntrat mig att 'tämja protonerna'. Du har hjälpt mig att hitta lagom, att ha den balans jag behöver mellan liv och jobb. Och du gör mig lycklig. Du och vårt son David. Trots min kärlek för fysik och forskning, först och främst älskar jag er, Pär och David. David, mi cielo, mi lucero ... tus risas hacen que mis preocupaciones se evaporen y se me olvide que existe el tiempo. Tú eres mi fuente de energía y de felicidad. Sin vosotros dos, esta tesis hubiera perdido su significado.

# Bibliography


Belli M, Bettega D, Calzolari P, Cera F, Cherubini R, Dalla Vecchia M, Durante M, Favaretto S, Gialanella G, Grossi G, Marchesini R, Moschini G, Piazzola A, Poli G, Pugliese M, Sapora O, Scampoli P, Simone G, Sorrentino E, Tabocchini M A, Tallone L, and Tiveron P 2000 Inactivation of human normal and tumour cells irradiated with low energy protons *Int. J. Radiat. Biol.* **76** 831–39

Belli M, Cherubini R, Dalla Vecchia M, Dini V, Esposito G, Moschini G, Sapora O, Simone G and Tabocchini M A 2002 DNA fragmentation in V79 cells irradiated with light ions as measured by pulsed-field gel electrophoresis. I. Experimental results *Int. J. Radiat. Biol.* **78** 475–82

Benedito E, Fernández-Varea J M, and Salvat F 2001 Mixed simulation of the multiple elastic scattering of electrons and positrons using partial-wave differential cross-sections *Nucl. Instrum. Methods Phys. Res. B* **174** 91–110

Berger M J 1963 Monte Carlo calculation of the penetration and diffusion of fast charged particles *Methods Comp. Phys.* **1** 135–215

Bigildeev E A and Michalik V 1996 Charged particle tracks in water of different phases. Monte Carlo simulation of electron tracks *Radiat. Phys. Chem.* **47** 197–207

Bote D and Salvat F 2008 Calculations of inner-shell ionization by electron impact with the distorted-wave and plane-wave Born approximations *Phys. Rev. A* **77** 042701

Brahme A 2004 Recent advances in light ion radiation therapy *Int. J. Radiation Oncology Biol. Phys.* **58** 603–16

Bues M, Newhauser W D, Titt U and Smith A R 2005 Therapeutic step and shoot proton beam spot-scanning with a multi-leaf collimator: a Monte Carlo study. *Radiat. Protect. Dosim.* **115** 164–9

Campa A, Esposito G, Belli M, Simone G and Tabocchini M A 2004 DNA fragmentation in V79 cells irradiated with light ions as measured by pulsed-field gel electrophoresis. II. Simulation with a generalized broken stick model *Int. J. Radiat. Biol.* **80** 229–238

Champion C, L'Hoir A, Politis M F, Fainstein P D, Rivarola R D and Chetioui A 2005 A Monte Carlo Code for the simulation of heavy-ion tracks in water *Radiat. Res.* **163** 222–31

Champion C and Loirec C Le 2006 Positron follow-up in liquid water: I. A new Monte Carlo track-structure code *Phys. Med. Biol.* **51** 1707–23

Charlton D E, Goodhead D T, Wilson W E, and Paretzke H G 1985 The deposition of energy in small cylindrical targets by high LET radiations *Radiat. Protect. Dosim.* **13** 123–25

Chen J, Kellerer A M and Rossi H H 1994 Radially restricted linear energy transfer for high-energy protons: a new analytical approach *Radiat. Environ. Biophys.* **33** 181–7

Cucinotta F A, Katz R and Wilson J W 1998 Radial distribution of electron spectra from high-energy ions *Radiat. Environ. Biophys.* **37** 259–65

Dahm R 2008 Discovering DNA: Friedrich Miescher and the early years of nucleic acid research *Hum. Gen.* **122** 565–81

Dingfelder M, Hantke D, Inokuti M and Paretzke H G 1998 Electron inelastic-scattering cross sections in liquid water *Radiat. Phys. Chem.* **53** 1–18

Dingfelder M, Inokuti M and Paretzke H G 2000 Inelastic-collision cross sections of liquid water for interactions of energetic protons *Radiat. Phys. Chem.* **59** 255–75

Dingfelder M, Ritchie R H, Turner J E, Friedland W, Paretzke H G and Hamm R N 2008 Comparisons of calculations with PARTRAC and NOREC: transport of electrons in liquid water *Radiat. Res.* **169** 584–94

Dingfelder M 2013 Updated model for dielectric response function of liquid water *App. Radiat. Isotopes* (In press)

DSMF 2013 Danish Society for Medical Physics http://www.dsmf.org/, http://www.dsmf-symposium.dk/

Emfietzoglou D, Cucinotta F A and Nikjoo H 2005 A complete dielectric response model for liquid water: a solution of the Bethe ridge problem *Radiat. Res.* **164** 202–11

Elsässer T, Krämer M and Scholz M 2008 Accuracy of the local effect model for the prediction of biologic effects of carbon ion beams in vitro and in vivo *Int. J. Radiat. Oncology Biol. Phys.* **71** 866–72

Emfietzoglou D, Karava K, Papamichael G and Moscovitch M 2003 Monte Carlo simulation of the energy loss of low-energy electrons in liquid water *Phys. Med. Biol.* **48** 2355–71

Emfietzoglou D, Karava K, Papamichael G and Moscovitch M 2004 Monte Carlo calculations of radial dose and restricted-LET for protons in water *Radiat. Prot. Dosim.* **110** 871–9

Falkmer S, Fors B, Larsson B, Lindell A, Naeslund J and Stenson S 1962 Pilot study on proton irradiation of human carcinoma *Acta Radiol. Therapy Physics Biology* **58** 33–51

Friedland W, Dingfelder M, Jacob P and Paretzke H G 2005 Calculated DNA double-strand break and fragmentation yields after irradiation with He ions *Radiat. Phys. Chem.* **72** 279–86

Friedrich T, Scholz U, Elsässer T, Durante M, and Scholz M 2012 Calculation of the biological effects of ion beams based on the microscopic spatial damage distribution pattern *Int. J. Radiat. Biol.* **88** 103–107

Goodhead D 2006 Energy deposition stochastics and track structure: what about the target? *Radiat. Protect. Dosim.* **122** 3–15

Grosswendt B 2006 Nanodosimetry, the metrological tool for connecting radiation physics with radiation biology *Radiat. Protect. Dosim.* **122** 404–14

Heller Jr. J M, Hamm R N, Birkhoff R D, and Painter L R 1974 Collective oscillation in liquid water *J. Chem. Phys.* **60** 3474–82

Holzscheiter M H, Bassler N, Dosanjh M, Sørensen B S, and Overgaard J 2012 A community call for a dedicated radiobiological research facility to support particle beam cancer therapy *Radiother. Oncol.* **105** 1–3

ICRU International Commission on Radiation Units and Measurements 1993 Stopping Powers and Ranges for Protons and Alpha Particles *ICRU Report 49* (Bethesda, MD: ICRU)

ICRU International Commission on Radiation Units and Measurements 1996 Secondary Electron Spectra from Charged Particle Interactions *ICRU Report 55* (Bethesda, MD: ICRU)

ICRU International Commission on Radiation Units and Measurements 1998 Fundamental Quantities and Units for Ionizing Radiation *ICRU Report 60* (Bethesda, MD: ICRU)

ICRU International Commission on Radiation Units and Measurements 2005 Stopping of ions heavier than helium *ICRU Report 73* (Bethesda, MD: ICRU)

ICRU International Commission on Radiation Units and Measurements 2007 Elastic Scattering of Electrons and Positrons *ICRU Report 77* (Bethesda, MD: ICRU)

ICRU International Commission on Radiation Units and Measurements 2007 Prescribing, Recording, and Reporting Proton-Beam Therapy *ICRU Report 78* (Bethesda, MD: ICRU)

Jakob B, Scholz M and Taucher-Scholz G 2002 Characterization of CDKN1A(p21) binding to sites of heavy-ion-induced damage: colocalization with proteins involved in DNA repair *Int. J. Radiat. Biol.* **78** 75–88

Jeggo P A 1998 Identification of genes involved in repair of DNA double-strand breaks in mammalian cells *Radiat. Res.* **150** S80-91

Johansson J 2006 Comparative treatment planning in radiotherapy and clinical impact of proton relative biological effectiveness *Doctoral Dissertation* Uppsala University

Karlsson K 2006 Role of non-homologous end-joining in repair of radiation-induced DNA double-strand breaks *Doctoral Dissertation* Uppsala University

Kempe J, Gudowska I and Brahme A 2006 Depth absorbed dose and LET distributions of therapeutic $^{1}$H, $^{4}$He, $^{7}$Li and $^{12}$C beams *Med. Phys.* **34** 183–92

Kempe J 2008 Development of analytical transport methods for biologically optimized light ion therapy *Doctoral Dissertation* Stockholm University

Kimstrand P 2008 Beam modelling for treatment planning of scanned proton beams *Doctoral Dissertation* Uppsala University

Kraft G, Krämer M and Scholz M 1992 LET, track structure and models *Radiat. Environ. Biophys.* **31** 161–80

Kraft G 2000 Tumor therapy with heavy charged particles *Prog. Part. Nucl. Phys.* **45** S473–S544

Liamsuwan T 2012 Development of Monte Carlo track structure simulations for protons and carbon ions in water *Doctoral Dissertation* Stockholm University

Lorin S 2008 Development of a compact scanning system *Licenciate Dissertation* Uppsala University

Medin J 1997 Studies of clinical proton dosimetry using Monte Carlo simulation and experimental techniques *Doctoral Dissertation* Stockholm University

Miller J H and Green A E S 1973 Proton energy degradation in water vapor *Radiat. Res.* **54** 343–63

Mould R F and Tai T H P 2002 Nasopharyngeal carcinoma: Treatments and outcomes in the 20th century *British J. Radiol.* **75** 307–39

Nikjoo H, Emfietzoglou R, Watanabe R, and Uehara S 2008 Can Monte Carlo track structure codes reveal reaction mechanism in DNA damage and improve radiation therapy? *Radiat. Phys. Chem.* **77** 1270–79

Nikjoo H, O'Neill P, Terrissol M and Goodhead D T 1999 Quantitative modelling of DNA damage using Monte Carlo track structure method *Radiat. Environ. Biophys.* **38** 31–8

Nikjoo H, Terrissol M, Hamm R N, Turner J E, Uehara S, Paretzke H G, and Goodhead D T 1994 Comparison of energy deposition in small cylindrical volumes by electrons generated by Monte Carlo track structure codes for gaseous and liquid water *Radiat. Prot. Dosim.* **52** 165–69

Nikjoo H, Uehara S, Emfietzoglou D and Cucinotta F A 2006 Track-structure codes in radiation research *Radiat. Meas.* **41** 1052–74

Ohsawa D, Sato Y, Okada Y, Shevelko V P and Soga F 2005 6.0–10.0-MeV/u $He^{2+}$-ion-induced electron emission from water vapor *Phys. Rev.* A **72** 062710

Ottolenghi A, Merzagora M and Paretzke H G 1997 DNA complex lesions induced by protons and $\alpha$-particles: track structure characteristics determining linear energy transfer and particle type dependence *Radiat. Environ. Biophys.* **36** 97–103

Paganetti H and Goitein M 2000 Radiobiological significance of beamline dependent proton energy distributions in a spread-out Bragg peak *Med. Phys.* **27** 1119–26

PTCOG 2013 Particle Therapy Co-operative Group http://ptcog.web.psi.ch/

Qiang L and Zengquan W 1997 Calculations of heavy ion track structure and energy deposition distribution in liquid water *Nucl. Instrum. Meth. B* **122** 657–62

Sachs R K, Chen A M and Brenner D J 1997 Review: Proximity effects in the production of chromosome aberrations by ionizing radiation *Int. J. Radiat. Biol.* **71** 1–19

Safai S, Bortfeld T and Engelsman M 2008 Comparison between the lateral penumbra of a collimated double-scattered beam and uncollimated scanning beam in proton therapy *Phys. Med. Biol.* **53** 1729–50

Salvat F, Jablonski A and Powell C 2005 ELSEPA—Dirac partial-wave calculation of elastic scattering of electrons and positrons by atoms, positive ions and molecules *Comput. Phys. Comm.* **165** 157–90

Salvat F, Fernández-Varea J M and Sempau J 2008 PENELOPE-2008: A Code System for Monte Carlo Simulation of Electron and Photon Transport (OECD Nuclear Energy

Agency, Issy-les-Moulineaux)
Schardt D, Elsässer T, and Schulz-Ertner D 2010 Heavy-ion tumor therapy: Physical and radiobiological benefits *Rev. Mod. Phys.* **82** 383–425
Seltzer S M and Berger M J 1986 Bremsstrahlung energy spectra from electrons with kinetic energy 1 keV–10 GeV incident on screened nuclei and orbital electrons of neutral atoms with $Z = 1$–100 *At. Data Nucl. Data Tables* **35** 345–418
Skandionkliniken 2013 http://www.skandionkliniken.se/
Stenerlöw B, Höglund E, Elmroth K, Karlsson K H and Radulescu I 2002 Radiation quality dependence of DNA damage induction *Radiat. Prot. Dosim.* **99** 137–41
Stenerlöw B, Pettersson O A, Essand M, Blomquist E, and Carlsson J 1995 Irregular variations in radiation sensitivity when the linear energy transfer is increased *Rad. Oncol.* **36** 133–42
Stolterfoht N, DuBois R D and Rivarola R D 1997 Electron Emission in Heavy Ion-Atom Collisions (Springer: Berlin)
Tilly N 2002 Radiobiological investigations of proton and light ion therapy *Doctoral dissertation* Stockholm University
Tobias Böhlen T 2012 Monte Carlo particle transport codes for ion beam therapy treatment planning: Validation, development and applications *Doctoral Dissertation* Stockholm University
Tobias C A, Roberts J E, Lawrence J H, Low-Beer B V A, Anger H O, Born J, McCombs R, and Huggins C 1956 Irradiation of hypophysectomy and related studies using 340 MeV protons and 190 MeV deuterons *Peaceful Uses Atom. Energy* **10** 95–106
Uehara S, Toburen L H and Nikjoo H 2001 Development of a Monte Carlo track structure code for low-energy protons in water *Int. J. Radiat. Biol.* **77** 139–54
Uehara S and Nikjoo H 2002 Track structure for low energy ions including charge exchange processes *Radiat. Prot. Dosim.* **99** 53–5
Wambersie A, Deluca P M, Andreo P, and Hendry J H 2004 'Light' or 'Heavy' ions: A debate of terminology? *Radiotherapy Oncol.* **73** suppl.2
Weyrather W K, Ritter S, Scholz M, and Kraft G 1999 RBE for carbon track-segment irradiation in cell lines of differing repair capacity *Int. J. Radiat. Biol.* **75** 1357–64
Wilson R R 1946 Radiological use of fast protons *Radiology* **47** 487–91

Acta Universitatis Upsaliensis

*Digital Comprehensive Summaries of Uppsala Dissertations from the Faculty of Medicine* 930

Editor: The Dean of the Faculty of Medicine

A doctoral dissertation from the Faculty of Medicine, Uppsala University, is usually a summary of a number of papers. A few copies of the complete dissertation are kept at major Swedish research libraries, while the summary alone is distributed internationally through the series Digital Comprehensive Summaries of Uppsala Dissertations from the Faculty of Medicine.

Distribution: publications.uu.se
urn:nbn:se:uu:diva-206385

ACTA
UNIVERSITATIS
UPSALIENSIS
UPPSALA
2013